IMPERIAL COLLEGE LONDON

THEORETICAL PHYSICS GROUP

Gertsenshtein Mechanism and its Potential Applications in Gravitational Waves Detection

MSC DISSERTATION

Author:
Jean Luo

Supervisor:
Prof. Carlo Contaldi

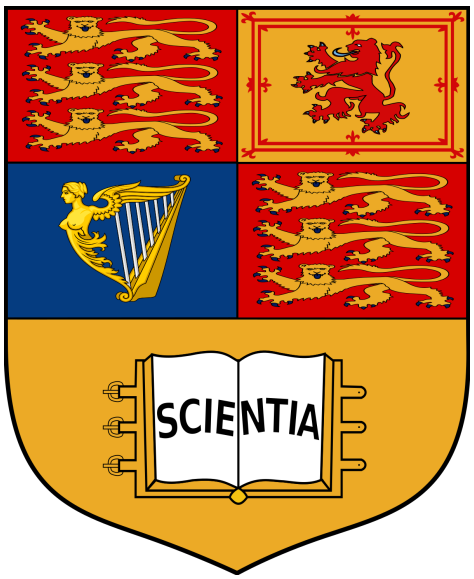

Submitted in partial fulfillment of the requirements for the MSc degree in Quantum Fields and Fundamental Forces of Imperial College London

Sep 2024

Abstract

The (inverse) Gertsenshtein mechanism is a direct consequence of general relativity, which describes the mutual conversion of photons and gravitons in the presence of a background magnetic field. The fact of being a frequency independent process enables the applications of the (inverse) Gertsenshtein mechanism to detect gravitational waves in frequency ranges beyond the reach of the current ground-based detectors ($\gtrsim 10$kHz), which makes this mechanism an unique probe to early universe physics and high energy physics beyond the Standard Model. This work aims to provide the very first review of this particular mechanism and its potential applications in the detection of high-frequency gravitational waves (HFGWs), which starts from an introduction to key theoretical concepts of gravitational waves in general relativity and the current observations process for completeness, which is followed by a qualitative discussion of potential sources of HFGWs. The major part of this work is a detailed construction of an unified theoretical and mathematical framework of the (inverse) Gertsenshtein mechanism along with some phenomelogical results for concrete cosmological/astrophysical examples. While starting from a toy model in vacuum to provide some intuitive insight, a more realistic cosmological scenario incorporating plasma/QED/optical effects is discussed in details by solving the coupled differential equations both in the WKB approximation and exactly for homogeneous background magnetic field, a discussion of the perturbative treatment of inhomogeneous magnetic field is also introduced. The dissertation is then closed by providing some phenomenological and experimental insight into its potential applications in both indirect (CMB distortion observations) and direct (laboratory experiments) detection possibilities of HFGWs.

Acknowledgments

J.L. would like to express his gratitude towards Prof. Carlo Contaldi for the supervision, the timely helps and the selection of this frontier topic currently under rapid development tailored for J.L.'s academic interests and background.

J.L.'s thanks and appreciations also go to his parents for both the mental and financial supports.

Besides, J.L is grateful to his friends and colleagues Muchen, Jizhe, Hunter, Roger and Yifan for accompanying J.L. throughout the intense study of theoretical physics at Imperial College London.

List of abbreviated names of experiments

ACT: Atacama Cosmology Telescope

ALPS: Any Light Particle Search

ARCADE2: Second-generation Absolute Radiometer for Cosmology, Astrophysics, and Diffuse Emission

BAUSCIA: Bulk Acoustic Wave Sensors for High-frequency Antenna

CAST: CERN Axion Solar Telescope

EDGES: Experiment to Detect the Global EoR Signature

EPTA: European Pulsar Timing Array

LHC: Large Hadron Collider

LIGO: Laser Interferometer Gravitational-Wave Observatory

LISA: Laser Interferometer Space Antenna

KAGRA: Large-scale Cryogenic Gravitational Wave Telescope

MAGE: Multimode Acoustic Gravitational Wave Experiment

MAGO: Microwave Apparatus for Gravitational waves Observation

NANOGrav: North American Nanohertz Observatory for Gravitational Waves

OSQAR: Optical Search for QED Vacuum Bifringence, Axions and Photon Regeneration

PPTA: Parkes Pulsar Timing Array

Contents

Chapter 1

Introduction

1.1 Background

After the historical success of LIGO and Virgo collaborations in 2015 for the direct detection of the first gravitational wave event GW150914 from a merger event of binary black holes in humanity's history [1], the study of gravitational waves, from either the theoretical or the observational aspects, has become one of the main focuses of the modern fundamental physics.

The gravitational waves propagating in the universe have very distinct origins and hence are emitted in a very large range of frequency. However, the nature of interferometry method employed by LIGO, and other similar detectors such as VIRGO, limits its sensitive frequency range of gravitational wave signals to only the low frequency band of $\lesssim 10$kHz due to the influence of the laser shot noise, and the other detectors such as Pulsar Timing arrays (PTAs) and space-based interferometers all probe in even lower frequency range $\lesssim 1$Hz. Such difficulties leave gravitational waves in the higher frequency band undetected. Therefore, the strategy of detecting high frequency gravitational waves (HFGWs), especially ultra-high frequency gravitational waves (UHFGWs) of frequency band higher than MHz, remains a research area under active development and debate.

The potential sources of such energetic gravitational waves are mostly likely to be phenomena related to physics beyond the Standard Model of Particle Physics, such as topological defects due to the presence of string or magnetic monopoles, or extreme cosmological/astrophysics events, such as primordial black holes or early universe phase transitions [2; 3; 4]. Hence, the study of HFGWs could provide unique and invaluable insight into the development of fundamental physics in almost all aspects.

A potential solution to the detection of HFGWs is the applications of the (inverse) Gertsenshtein effect [5], which was first proposed in 1962 and states that in a curved spacetime, electromagnetic waves can be converted into gravitational waves with the presence of a background magnetic field. In the 70s, the inverse process, i.e the gravition-photon conversion, which was described as "hardly of interest" in Gertsen-

shtein's original paper [5], was studied as well. People at the time considered it as potential tools of detecting gravitational waves [6; 7; 8], both in artificial laboratory environments by producing the gravitational waves using photons and in astrophysical/cosmological environment by astronomical instruments [6; 7; 9].

In recent years, the (inverse) Gertsenshtein mechanism has re-attracted increasing attention in its applications in the detection of ultra-high frequency gravitational waves (UHF-GWs) and cosmological constraints [2; 10; 9], since the technological development has enabled the direct detection of HFGWs using existing facilities (such as the axion detectors built in recent years) or new gravitational wave detectors specifically designed for this purpose [2; 9; 10; 11].

1.2 Report structure

The dissertation is organised as followed. In Chapter 2, we start from the theoretical formalism of gravitational waves in the framework of general relativity along with a toy binary merger model illustrating how gravitational radiation is produced, which is followed by a brief introduction to the major gravitational waves detectors that are operating or under construction. In Chapter 3, a qualitative review of the most studied sources of HFGWs is provided for completeness (mainly) from both the astrophysical (primordial black holes) and cosmological (evolution of the early universe) aspects, with a particular focus on the strain or/and stochastic energy density spectrum they induce.

In Chapter 4, we provide a modern formalism of the Gertsenshtein mechanism, concentrating on a detailed derivation of the graviton-photon conversion process in vacuum for constant magnetic, along with a discussion of the treatment of electric and magnetic field in curved spacetime. In Chapter 5, we continue the efforts in Chapter 4 by incorporating extra plasma/QED/optical effects that would appear in actual modelling of astrophysical or cosmological scenarios, some concrete examples with a hierarchy of scales are provided.

In Chapter 6, the distortions of the CMB background due to Gertsenshtein effect and how could they be detected by radiotelescopes are investigated, which could be a form of indirect detection of HFGWs and are compared to parallel effects that also distort the CMB. In Chapter 7, we focus on the laboratory experiments different to the ones introduced in Chapter 2, which have the potential to directly detect HFGWs and are compared to a couple of other HFGWs detectors based on different principles. In Chapter 8, we summarise the results and discuss the potential future development of the HFGWs based on the Gerstenshtein effect.

Chapter 2

Gravitational waves and the progress on their detection

This chapter starts with the basic formalism of gravitational waves accompanied by a example of how a toy binary system generates gravitational radiation and a summary of the current observational progress of their detection. Due to length limit of the dissertation and the breadth of the research in gravitational waves, the emphasis will be given to results and discussions directly relevant to topics about Gertsenshtein mechanism in later chapters, such as stochastic gravitational wave backgrounds.

2.1 Formalism of gravitationl waves

2.1.1 Linearised gravity

In general relativity, only a very limited number of exact solutions that involve particular symmetries are known, such as the Schwarzschild solution implied by spherical symmetry in vacuum. However, interesting results can be obtained from approximations, among which a commonly used approximation is the linearised gravity. In this framework, we consider the usual line element

$$ds^2 = g_{\mu\nu}dx^\mu dx^\nu, \tag{2.1}$$

with the metric $g_{\mu\nu}$ of the particular form

$$g_{\mu\nu} = \eta_{\mu\nu} + h_{\mu\nu}, \tag{2.2}$$

where the tensorial perturbation $h_{\mu\nu}$ to the background Minkowski metric $\eta_{\mu\nu} = \text{diag}(-1, 1, 1, 1)$ is assumed to be small: $|h_{\mu\nu}| \ll 1$ (hence we always work in the leading order of perturbation). Despite behaving like a tensor in Lorentz transformations, $h_{\mu\nu}$ is not a tensor when considering general coordinate transformations. The indices of $h_{\mu\nu}$ are lowered/raised by $\eta_{\mu\nu}/\eta^{\mu\nu}$, so that the inverse metric takes the form

$$g^{\mu\nu} = \eta^{\mu\nu} - h^{\mu\nu}. \tag{2.3}$$

The Christoffel symbol $\Gamma^{\mu}_{\rho\sigma}$ is linearised as

$$\begin{aligned}\Gamma^{\mu}_{\rho\sigma} =& \frac{1}{2}(n^{\mu\nu}+h^{\mu\nu})[(n_{\nu\rho}+h_{\nu\rho})_{,\sigma}+(n_{\nu\sigma}+h_{\nu\sigma})_{,\rho}-(n+h_{\rho\sigma})_{,\nu}] \\ =& \frac{1}{2}\eta^{\mu\nu}(h_{\nu\rho,\sigma}+h_{\nu\sigma,\rho}-h_{\rho\sigma,\nu})+O(h^2),\end{aligned} \tag{2.4}$$

up to the leading order in $h_{\mu\nu}$. By ignoring $\Gamma\Gamma$ terms that are at least second order in perturbation, the linearised Riemann tensor $R_{\mu\nu\rho\sigma}$ becomes

$$\begin{aligned}R_{\mu\nu\rho\sigma}=\eta_{\mu\lambda}R^{\lambda}_{\nu\rho\sigma} =& \eta_{\mu\eta}(\Gamma^{\lambda}_{\sigma\nu,\rho}-\Gamma^{\lambda}_{\rho\nu,\sigma})+O(h^2) \\ =& \frac{1}{2}\eta_{\mu\lambda}\eta^{\lambda\gamma}(h_{\gamma\sigma,\nu\rho}+h_{\rho\nu,\gamma\sigma}-h_{\sigma\nu,\gamma\rho}-h_{\gamma\rho,\nu\sigma})+O(h^2) \\ =& \frac{1}{2}(h_{\mu\sigma,\nu\rho}+h_{\rho\nu,\mu\sigma}-h_{\sigma\nu,\mu\rho}-h_{\mu\rho,\nu\sigma})+O(h^2).\end{aligned} \tag{2.5}$$

Hence the Ricci tensor $R_{\mu\nu}=\eta^{\rho\sigma}R_{\rho\mu\sigma\nu}$ and the Ricci scalar $R=\eta^{\mu\nu}R_{\mu\nu}$ are respectively expressed as

$$R_{\mu\nu}=\frac{1}{2}(h^{\rho}_{\nu,\rho\mu}+h^{\rho}_{\mu,\rho\nu}-\Box h_{\mu\nu}-h_{,\mu\nu})+O(h^2), \tag{2.6}$$

$$R=h^{\mu\nu}_{,\mu\nu}-\Box h+O(h^2), \tag{2.7}$$

where $h\equiv h^{\alpha}_{\alpha}$. Finally, we can derive the Einstein tensor $G_{\mu\nu}$ and hence the Einstein equations in linearised gravity become

$$G_{\mu\nu}=8\pi GT_{\mu\nu}=\frac{1}{2}(h^{\rho}_{\nu,\rho\mu}+h^{\rho}_{\mu,\rho\nu}-\Box h_{\mu\nu}-h_{,\mu\nu}-\eta_{\mu\nu}h^{\mu\nu}_{\mu\nu}+\eta_{\mu\nu}\Box h)+O(h^2), \tag{2.8}$$

for some stress energy tensor $T_{\mu\nu}$.

2.1.2 Gauge symmetries

As a 4×4 symmetric matrix, $h_{\mu\nu}$ has seemingly ten independent elements without imposing gauge constraints. The equivalence of the Lorenz gauge in electromagnetism, the de Donder gauge, is commonly imposed to remove four degrees of freedom

$$\partial_{\mu}h^{\mu}_{\nu}-\frac{1}{2}\partial_{\nu}h=0. \tag{2.9}$$

However, there are still residual gauge freedom left after imposing the de Donder gauge, which can be removed from imposing the transverse-traceless (TT) gauge.

$$h=0 \quad \text{(traceless condition)} \tag{2.10}$$

$$h_{\mu\nu}u^{\mu}=0 \quad \text{(transverse condition)} \tag{2.11}$$

for some observer with 4-velocity u^{μ}. Up to a Lorentz transformation, the observer and the gravitational wave (propagating in z-direction) can always have a 4-velocity

$u^\mu = (1,0,0,0)$ and a 4-momentum $p^\mu = (E,0,0,E)$ for some constant E, respectively. Then the transverse condition implies that $h_{\mu 0} = 0$, and, together with the condition $h_{\mu\nu}k^\mu = 0$ implied by the de Donder gauge if every component of $h_{\mu\nu} = h_{\mu\nu}(t-z)$ behaves like a plane wave, we have $h_{\mu z} = 0$ as well. Therefore, the gravitational waves are left with only two physical polarisations. The resulting $h_{\mu\nu}$ takes the form

$$h_{\mu\nu} = \begin{pmatrix} 0 & 0 & 0 & 0 \\ 0 & h_+ & h_\times & 0 \\ 0 & h_\times & -h_+ & 0 \\ 0 & 0 & 0 & 0 \end{pmatrix}. \tag{2.12}$$

And the Einstein equations e.q. 2.8 are simplified to a very elegant form in TT gauge

$$\Box h_{\mu\nu} = -16\pi G T_{\mu\nu}, \tag{2.13}$$

which is a set of inhomogeneous wave equations.

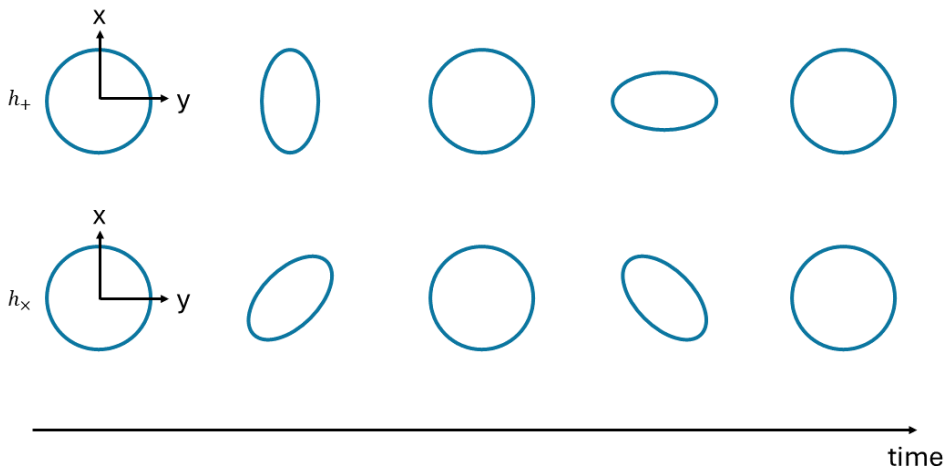

Figure 2.1: This diagram shows how a ring of test particles is deformed due to the gravitational waves with $+$ (top) and $\times$ (bottom) polarisations over time, where the deformation effects are highly exaggerated. The propagation direction of the gravitational waves is orthogonal to the paper.

As an aside, although there are only two physical polarisations in general relativity, more polarisations could exist in modified gravity theories due to the introduction of extra scalar/vector/tensor degrees of freedom. For example, in massive gravity, there are five physical polarisations, as expected for a massive spin-2 particle, where two of them are carried by a tensor, two of them are carried by a vector and one of them is carried by a scalar (the so-called fifth-force). The experimental search of such extra polarisations in current/proposed gravitational wave detection missions is of active interest.

2.1.3 Energy loss due to gravitational radiation

The inhomogeneous wave equations e.q. 2.8 can be solved via the Green's function technique, in analogy to solving the poison equation in electromagnetism, by considering the retarded influence of external source(s) due to causality

$$h_{\mu\nu}(t, \boldsymbol{x}) = 4G \int_{\Sigma} d^3y \frac{T_{\mu\nu}(t_r, \boldsymbol{y})}{|\boldsymbol{x} - \boldsymbol{y}|}, \tag{2.14}$$

where $t_r = t - |\boldsymbol{x} - \boldsymbol{y}|$ is the retarded time and Σ is the spatial region of the source. To simplify this solution, the size of the the region Σ is assumed to be much smaller than the distance d between the edge Σ and the object being influenced so that $d \sim |\boldsymbol{x} - \boldsymbol{y}| \sim$ constant. Meanwhile, it is also assumed the motion of the object is non-relativistic and the gravitational effects due the source are weak so that the approximated linearity is not broken [12]. Hence, e.q. 2.14 is simplified to

$$h_{\mu\nu}(t, \boldsymbol{x}) = \frac{4G}{d} \int_{\Sigma} d^3y T_{\mu\nu}(t - d, \boldsymbol{y}). \tag{2.15}$$

In the context of gravitational waves, we are usually interested in h_{ij} since these components are directly relevant to the experimentally measured quantities, such as the gravitational strain i.e. the length change caused by perturbation to flat spacetime. To convert T_{ij} in e.q. 2.15, the stress tensor, into a quantity easier to be modelled in actual observations, we employ the following mathematical tricks [12; 13]: by the conservation law $\partial_\mu T^{\mu\nu} = 0$, we have

$$\partial_\mu T^{\mu 0} = 0 \Rightarrow \partial_0^2 T^{00} = -\partial_k \partial_0 T^{k0} = \partial_k \partial_l T^{kl}. \tag{2.16}$$

Multiply both sides by $x^i x^j$ and integrate over Σ

$$\int_{\Sigma} x^i x^j \partial_0^2 T^{00}(t, \boldsymbol{x}) d^3x = \int_{\Sigma} x^i x^j \partial_k \partial_l T^{kl}(t, \boldsymbol{x}) d^3x = 2 \int_{\Sigma} T^{ij} d^3x, \tag{2.17}$$

which turns the integral over T^{ij} into an integral over T^{00}, the energy mass density of the source. By defining the quadrupole moment I_{ij}

$$I_{ij} = \int d^3x x^i x^j T^{00}, \tag{2.18}$$

e.q. 2.15 is expressed in terms of I_{ij} as

$$h_{ij}(t, r) = \frac{2G}{r} \frac{\partial^2}{\partial t^2} I_{ij}(t - r). \tag{2.19}$$

As will be seen from below, e.q. 2.19 is more conveniently expressed in terms of traceless quadrupole moment:

$$J_{ij} \equiv I_{ij} - \frac{1}{3} \delta_{ij} I_k^k, \tag{2.20}$$

such that

$$h_{ij}(t,r) = \frac{2G}{r}\frac{\partial^2}{\partial t^2}I_{ij}(t-r) = \frac{2G}{r}\frac{\partial^2}{\partial t^2}(J_{ij}(t-r) + \frac{1}{3}\delta_{ij}I^k_k(t-r)). \tag{2.21}$$

The fact that h_{ij} is determined by the quadrupole is physically valid: In general relativity, both monopole and dipole are constant due to the conservation of totol energy and momentum, respectively [14; 15]. Hence, by considering a multipole expansion of $h_{\mu\nu}$, the leading contribution to the gravitational radiation is indeed the quadrupole moment I_{ij} [14].

On the other hand, with the existence of gravitational radiation that significantly contributes to the total stress-energy, we need to consider the additional contribution from the Landau–Lifshitz pseudotensor $(-g)t^{LL}_{\mu\nu}$ that characterises the energy carried by gravitational field itself instead of only the non-gravitational stress-energy tensor $T_{\mu\nu}$ (by pseudotensor we mean a tensorial-like object that does not transform covariantly under diffeomorphism) [14]. Hence the Einstein equations e.q. 2.13 are generalised to relaxed Einstein equations of the form (in de Donder gauge)

$$\Box h_{\mu\nu} = -16\pi G\tau_{\mu\nu}, \tag{2.22}$$

where $\tau_{\mu\nu} = (-g)(T_{\mu\nu} + t^{LL}_{\mu\nu})$ is the total stress-energy of the system [14].
In the TT gauge, this Landau–Lifshitz pseudotensor can be simplified to

$$(-g)t^{\alpha\beta}_{LL} = \frac{1}{32\pi G}(\dot{h}^{ij}_T\dot{h}^T_{ij}T)s^\alpha s^\beta, \tag{2.23}$$

where $s = (1, \hat{x})$ is the null vector tangent to the geodesic of the gravitational wave propagating in the $\hat{x}$ (unit vector) spatial direction [14]. Physically, it is natural to express the energy flux due to gravitational radiation P in terms of the Landau–Lifshitz pseudotensor by considering the following integral over a 2-sphere in the far zone S^2_∞:

$$P = \int_{S^2_\infty}(-g)r^2 d\Omega\hat{\boldsymbol{x}}\cdot\boldsymbol{q}, \tag{2.24}$$

where $q^i = t^{0i}_{LL}$ is the density energy flux due to gravitational radiation. Hence substituteing e.q. 2.23 into this integral, we get an explicit expression of P in terms of polarisations of h_{ij} [14]

$$P = \frac{1}{16\pi G}\int d\Omega\left[\left(\frac{\partial}{\partial t}h_+\right)^2 + \left(\frac{\partial}{\partial t}h_\times\right)^2\right]r^2. \tag{2.25}$$

Further substituting e.q. 2.21 into e.q. 2.25, the energy loss can be expressed in terms of J_{ij}

$$\frac{dE}{dt} = -P = -\frac{G}{5}\left(\frac{\partial^3}{\partial t^3}J_{ij}\right)\left(\frac{\partial^3}{\partial t^3}J^{ij}\right). \tag{2.26}$$

2.1.4 A toy model for inspirals of compact binary

As a more concrete toy example for gravitational radiation, the inspiral of a binary system can be modelled by the following semi-classical model: consider an idealised binary system consisting of two identical objects of mass M separated by a distance $2l$, we assume this separation is much larger than the radius of the two objects and hence the effects due to the shape of the objects (e.g. tidal forces) are ignored. The motion of the two objects are considered to be initially within a circular orbit, when there is no energy loss due to gravitational radiation, in the xy-plane with initial conditions

$$\begin{aligned} \boldsymbol{x}_1(t=0) &= (l,0,0); \quad & \boldsymbol{x}_2(t=0) &= (-l,0,0); \\ \dot{\boldsymbol{x}}_1(t=0) &= (0,\omega l,0); \quad & \dot{\boldsymbol{x}}_2(t=0) &= (0,-\omega l,0), \end{aligned} \tag{2.27}$$

for angular velocity ω. The inspiral process is assumed to change the orbit distance very slowly.
By Newtonian mechanics, the total energy of the system is

$$E = 2\left(\frac{1}{2}M\omega^2 l^2 - \frac{G}{l}\left(\frac{M}{2}\right)^2\right), \tag{2.28}$$

and Newton's Second law implies

$$M\omega^2 l = \frac{GM^2}{(2l)^2} \Rightarrow \omega = \sqrt{\frac{GM}{4l^3}}, \tag{2.29}$$

hence

$$E = 2\left(\frac{GM^2}{8l} - \frac{GM^2}{4l}\right) = -\frac{GM^2}{4l}. \tag{2.30}$$

Assume that the energy radiated is small compared the rest mass of both objects, the energy flow is

$$\frac{dE}{dt} = \frac{GM^2}{4l^2}\frac{dl}{dt} = \frac{G}{5}\left(\frac{\partial^3}{\partial t^3}J_{ij}\right)\left(\frac{\partial^3}{\partial t^3}J^{ij}\right), \tag{2.31}$$

from the result in e.q. 2.26.
The initial conditions in e.q. 2.27 can be recast into the energy-mass density T^{00} [12]

$$T^{00}(t,\boldsymbol{x}) = M(\delta(x - l\cos\omega t)\delta(y - l\sin\omega t) + \delta(x + l\cos\omega t)\delta(y + l\sin\omega t))\delta(z). \tag{2.32}$$

Thus, by e.q. 2.18,

$$I_{ij} = Ml^2\begin{pmatrix} 1+\cos 2\omega t & \sin 2\omega t & 0 \\ \sin 2\omega t & 1-\cos 2\omega t & 0 \\ 0 & 0 & 0 \end{pmatrix} \tag{2.33}$$

$$\Rightarrow J_{ij} = \frac{1}{3}Ml^2\omega^3\begin{pmatrix} 1+3\cos 2\omega t & 3\sin 2\omega t & 0 \\ 3\sin 2\omega t & 1-3\cos 2\omega t & 0 \\ 0 & 0 & -2 \end{pmatrix} \tag{2.34}$$

$$\Rightarrow \frac{\partial^3}{\partial t^3} J_{ij} = 8Ml^2\omega^3 \begin{pmatrix} \sin 2\omega t & -\cos 2\omega t & 0 \\ -\cos 2\omega t & -\sin 2\omega t & 0 \\ 0 & 0 & 0 \end{pmatrix}. \tag{2.35}$$

Hence $J_{ij}J^{ij} = 128M^2l^4\omega^6$ and

$$\frac{dE}{dt} = \frac{128}{5} GM^2R^4\omega^6 \Rightarrow l^3\frac{dl}{dt} = -\frac{8}{5}G^3M^3. \tag{2.36}$$

This differential equation of $l(t)$ can be directly solved as

$$\int_0^l dl' l'^3 = -\frac{8}{5}G^3M^3 \int_t^{t_m} dt' \Rightarrow l(t) = \left[\frac{32}{5}\frac{G^3M^3}{c^5}(t_m - t)\right]^{\frac{1}{4}}, \tag{2.37}$$

where t_m is time for the merger event to occur and we have reintroduced the speed of light c in the last step by dimensional analysis in order to apply the result to numerical calculations related to actual astrophysical systems. Physically, e.q. 2.18 shows that the separation l indeed decreases with the time evolution due to the gravitational radiation, and $l \to 0$ as $t \to t_m$, i.e. when the coalescence occurs.

The gravitational wave frequency emitted by this binary system is twice the orbital frequency because for a binary system consisting of two nearly identical objects, completing every half-orbit turns the system into its original state. Therefore, the quadrupole moment of the oscillates at a period half to the orbit period. As mentioned previously, the gravitational wave is mostly induced by the variation of this quadrupole moment and hence the gravitational wave emitted by a binary system is twice of the orbital frequency of the latter [16; 17]. Thus, one can rearrange e.q. 2.18 to work out the gravitational wave frequency $f_{gw} = \frac{\omega}{\pi}$:

$$f_{\text{gw}}(t) = \frac{1}{8\pi}\left(250\left(\frac{c^3}{GM}\right)^5\left(\frac{1}{t_m - t}\right)^3\right)^{\frac{1}{8}}, \tag{2.38}$$

which increases with time evolution (i.e. as orbit lowers), and diverges as $t \to t_m$ and hence suggests that the coalescence is extremely powerful, which is too powerful to be described by this over-simplified semi-Newtonian model [15; 16]. A detailed description of the coalescence heavily depends on the specific binary system being studied, which involves strong relativistic effects and other factors when considering the exact shape of the objects, such as tidal disruption that might occur in the coalescence of two neutron stars [18].

Another relevant observable is the amplitude of $h_{\mu\nu}$, denoted as h_c, which could be directly derived by substituting e.q. 2.33 into e.q. 2.19:

$$h_c \approx \frac{8G^2M^2}{c^4rl}, \tag{2.39}$$

which is the dimensionless strain that is used for actual measurements to describe, e.g., the change in the arm length of an interferometer [18].

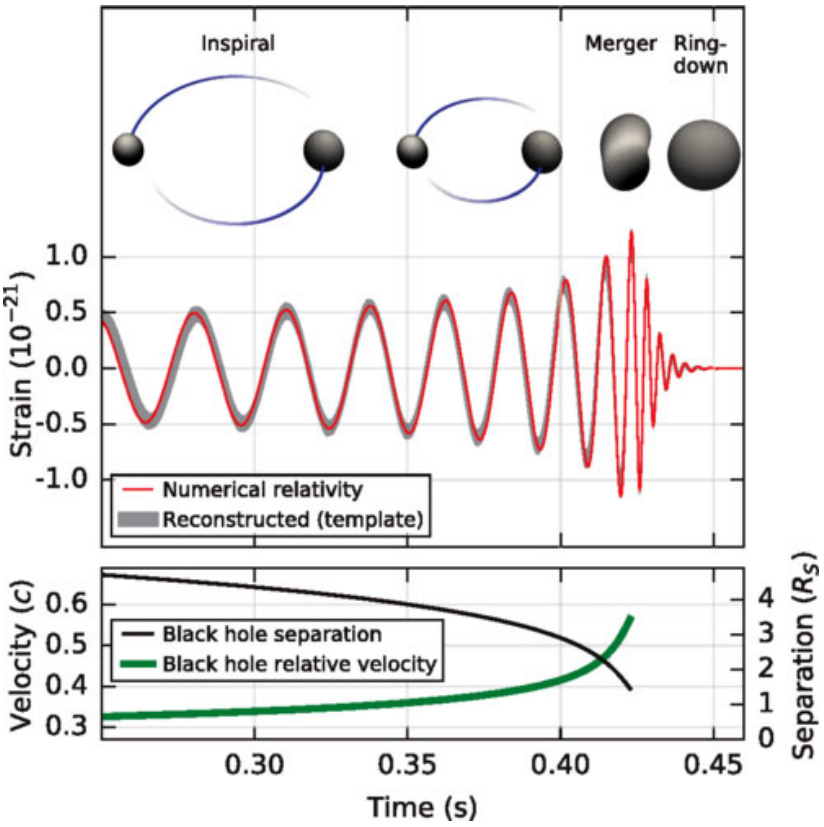

Figure 2.2: A diagram showing the inspiral, merger and ringdown stages of a binry system with two compact astrophysical objects (top). The idealised waveform without noises expected to see on gravitational wave detectors (middle) and the expected relative velocity & separation distance (bottom) at different stages are also shown. Diagram taken from [1].

Example: the Hulse-Taylor binary pulsar

A well-known example is the Hulse-Taylor binary pulsar, or PSR 1913+16, which was the first observed binary pulsar discovered in 1974 [19]. This binary system, around 6400pc away from us, consists of two neutron stars of almost equal mass $M \sim 1.4 M_S$ currently separated by a distance of $2l \sim 2 \times 10^6$km (approximation of an elliptical orbit) with a period of the orbital motion of roughly 8 hours [20], where $M_S \approx 2 \times 10^{30}$kg is the solar mass. Plugging in these numbers into e.q. 2.38 and e.q. 2.39, one get

$$f_{\text{gw,HT}}(t) \approx 1.46 \text{ Hz} \left(\frac{1 \text{ day}}{t - t_m} \right), \tag{2.40}$$

$$h_{c,\text{HT}} \sim 10^{-26}, \tag{2.41}$$

which is much lower than the typical detection range of LIGO or VIRGO which is around $h_c \sim 10^{-21}$ [15; 18].
Despite not being able to be directly detected, PSR 1913+16 served as the first indirect measurement of gravitational waves [20; 21], which is a landmark evidence for the existence of gravitational waves well before the discovery of LIGO in 2015. The

observed negative increase in the orbital period $\dot{P}_{b,obs}$, which was first measured in 1979 and improved in subsequent years, eventually matches the theoretical prediction $\dot{P}_{b,theo}$ to at a precision of 0.8%:

$$\frac{\dot{P}_{b,\text{obs}} - \dot{P}_{b,\text{gal}}}{\dot{P}_{b,\text{theo}}} = 0.997 \pm 0.002, \tag{2.42}$$

where $\dot{P}_{b,gal}$ accounts for the galactic accelerations and proper motion of the pulsar [20; 21; 22].

2.2 Stochastic gravitational wave background

Ideally, one would expect the signal from an event like the coalescence of a binary system to produce a coherent, i.e. a wave signal with a predictable waveform that could be constructively interfered to have a high signal-to-noise ratio that is detectable [18]. This situation was, for example, the case for the first detection of gravitational waves from binary black holes coalescence, the GW150914 event, the signal of which was compared to the existing theoretical prediction of the waveform in order to confirm the detection of the gravitational waves [1].

But in practice, it is very common to have incoherent gravitational signals being a mixture of multiple sources or emitted by irregular sources, which destructively interfere and hence produce weak signals [15]. These weak signals cannot be matched to the waveform of a particular event and behave randomly like noise backgrounds in the detectors. Hence we refer such signals as stochastic gravitational wave backgrounds (SGWBs) which could be studied as an additional contribution to the noise of the detector [15]. How to differentiate this noise contribution due to SGWBs from the other noise contributions in the detectors is an important research area under active development for future space-based interferometric detectors like LISA and TAIJI that are expected to have enough sensitivity to directly detect SGWBs.

The sources of SGWBs can be, on one hand, the astrophysical sources such as the binary systems mentioned previously which are usually too distant from us to produce a resolvable signal. On the other hand, it is believed that the main contributions are from cosmological sources, whereas the astrophysical sources serve as a foreground [23]. A typical source of stochastic waves is the inflation, since the quantum fluctuations make the metric perturbation a random variable, other examples involve cosmic strings and primordial black holes [23]. Such stochastic property is a familiar concept in cosmology, since the cosmic microwave background radiation (CMBR), a random distribution of relic photons from early universe, is in fact a stochastic electromagnetic wave background [23; 24].

Being a random variable means that the mathematical description of a stochastic wave must be statistical. Just as for CMBR, we study the frequency distribution of SGWBs by defining the dimensionless energy density spectrum Ω_{gw} in the following

normalisation [15; 23]:

$$\Omega_{\text{gw}}(f) \equiv \frac{1}{\rho_c}\frac{d\rho}{d\ln f}, \tag{2.43}$$

where ρ is the density of SGWBs and ρ_c is the critical density nowadays

$$\rho = \frac{3H_0^2}{8\pi G}, \tag{2.44}$$

for the present-day Hubble rate H_0.
Consider a perfect fluid with stress-energy tensor

$$T_{\mu\nu} = (\rho + p)u_\mu u_\nu + p g_{\mu\nu} \Rightarrow T_{00} = \rho, \tag{2.45}$$

with some pressure p and 4-vector of some observer $u = (-1, 0, 0, 0)$ up to an Lorentz transformation. Meanwhile, in linearised gravity, the stress-energy tensor is also define by the metric perturbations as

$$T_{\mu\nu} \equiv \frac{1}{32\pi G}\langle \partial_\mu h_{\rho\sigma} \partial_\nu h^{\rho\sigma *} \rangle, \tag{2.46}$$

where $\langle ... \rangle$ represents the time average [25].

To proceed, expand h_{ij} into plane waves of continuous frequency on a sphere with solid angle Ω:

$$h_{ij}(t, \boldsymbol{x}) = \int_{-\infty}^{\infty} df \int d^2\Omega \sum_\lambda h_\lambda(f, \hat{\Omega}) \epsilon_{ij}^\lambda(\hat{\Omega}) e^{i2\pi f(t - \hat{\Omega}\cdot\boldsymbol{x})}, \tag{2.47}$$

where $\lambda = \{+, \times\}$ is the polarisation index, $\hat{\Omega}$ is the direction in which the gravitational wave propagates, $h_\lambda(f, \hat{\Omega})$ are the Fourier modes of h_{ij} with property $h_\lambda(f, \hat{\Omega}) = h_\lambda(-f, \hat{\Omega})^*$ since $h_{ij}(t, \boldsymbol{x})$ is real [15; 24]. We choose to work in the polarisation tensor basis ϵ_{ij}^λ such that

$$\epsilon^+(\hat{\Omega}) = \hat{e}_\theta \otimes \hat{e}_\theta - \hat{e}_\phi \otimes \hat{e}_\phi, \tag{2.48}$$

$$\epsilon^\times(\hat{\Omega}) = \hat{e}_\theta \otimes \hat{e}_\phi + \hat{e}_\phi \otimes \hat{e}_\theta, \tag{2.49}$$

where $\hat{e}_\theta$ and $\hat{e}_\phi$ are two orthonormal unit vectors spanning the plane orthogonal to $\hat{\Omega}$, defined as

$$\hat{e}_\theta = (\cos(\theta)\cos(\phi), \cos(\theta)\sin(\phi), -\sin\theta), \tag{2.50}$$

$$\hat{e}_\phi = (-\sin(\phi), \cos(\phi), 0), \tag{2.51}$$

for the usual polar and azimuthal angles θ and ϕ for a 2-sphere [24; 25]. Therefore, to compute the T^{00} component and hence ρ, we use the result $\partial_0 h_{ij} = i2\pi f h_{ij}$ from the plane wave assumption and hence

$$\begin{aligned} \partial_0 h_{ij} =& i2\pi f h_{ij} \\ \Rightarrow \langle \partial_0 h_{ij} \partial_0 h_{ij}^* \rangle =& 4\pi^2 \left(\int_{-\infty}^{\infty} df \int d^2\Omega \sum_\lambda \right) \left(\int_{-\infty}^{\infty} df' \int d^2\Omega' \sum_\lambda \right) f f' \end{aligned} \tag{2.52}$$

$$\times \langle h_\lambda(f,\hat{\Omega}) h_\lambda(f',\hat{\Omega}')\rangle e^{i2\pi f(t-\hat{\Omega}\cdot\boldsymbol{x})} e^{i2\pi f'(t-\hat{\Omega}'\cdot\boldsymbol{x})}. \tag{2.53}$$

If we assume that the SGWBs are isotropic, unpolarised and stationary, then

$$\langle h_\lambda(f,\hat{\Omega})\rangle = 0, \tag{2.54}$$

$$\langle h_\lambda(f,\hat{\Omega}) h_\lambda(f',\hat{\Omega}')\rangle = \delta_{\lambda\lambda'}\delta(f-f')\delta^2(\hat{\Omega}-\hat{\Omega}')S_{gw}(f), \tag{2.55}$$

where $\delta^2(\hat{\Omega}-\hat{\Omega}') \equiv \delta(\phi-\phi')\delta(\cos(\theta)-\cos(\theta'))$ [24; 25] represents isotropy, $\delta_{\lambda\lambda'}$ and $\delta(f-f')$ respectively represent the background being unpolarised and stationary, and $S_{gw}(f)$ is the power spectral density which is only frequency dependent due to isotropy. Substitute e.q. 2.55 into e.q. 2.53,

$$\rho = \frac{\pi}{8G}\int_{-\infty}^{\infty} df\, S_{gw}(f) f^2, \tag{2.56}$$

and hence e.q. 2.43 gives an explicit form in terms of f

$$\begin{aligned} H_0^2\Omega_{\text{gw}}(f) =& \frac{1}{\rho_c}\frac{\pi}{8G} f^3 S_{gw}(f) \\ =& \frac{\pi^2}{3} f^3 S_{gw}(f), \end{aligned} \tag{2.57}$$

which is often reexpressed in terms of the characteristic strain

$$h_c = \left(\frac{3H_0^2}{4\pi^2 f^2}\Omega_{\text{gw}}\right)^{\frac{1}{2}}. \tag{2.58}$$

2.3 Current progress on the detection of gravitational waves

2.3.1 Ground based interferometer

The current ground based gravitational wave interferometers, namely LIGO [26] in US, Virgo [27] in Italy and KAGRA [28] in Japan (known as LVK in combination), as well as the next-generation ones in construction like Einstein Telescope [29] in Europe and Cosmic Explorer [30] in US, all share similar design based on the Michelson interferometer. Each of these detectors consists of two perpendicular arms of kilometers long (e.g. $L = 3-4$ km for LVK) with a highly reflective mirror at the end of each arm, where the two arms are jointed by a beam splitter. A laser sources constantly send light beams into this beam splitter that split the beams into the two arms to measure the length of the latters.

When a gravitational passes through the interferometer, the induced spacetime perturbation changes the arm lengths and hence causes a relative phase shift in the

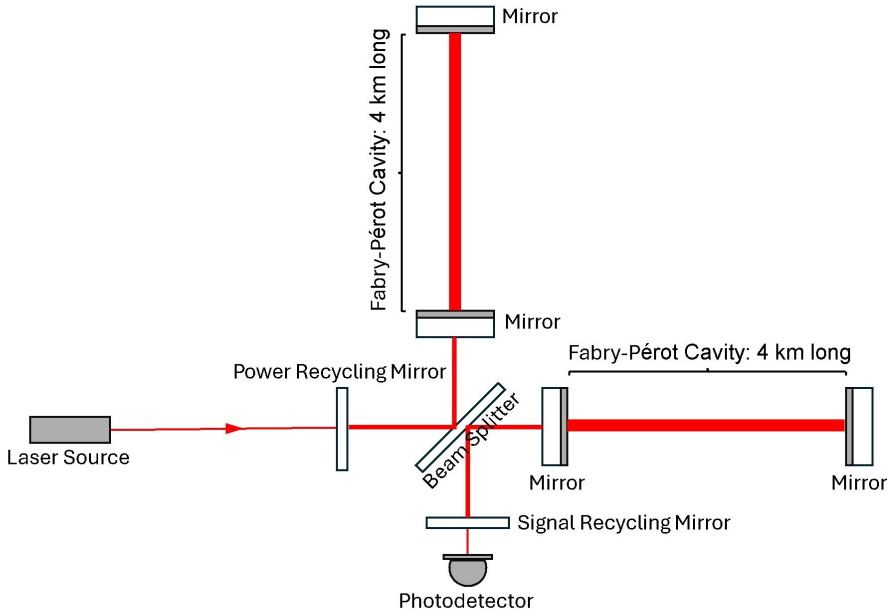

Figure 2.3: A simplified diagrammatic illustration of the design of LIGO, The two arms are two Fabry-Perot cavities that can further amplify the laser reflected by/passing through the beam splitter. Before hitting the beam splitter or being captured by the photodetector, the laser signals are amplified by a recycling mirror.

reflected light signals from the two arms, which can be measured by the photodetector to confirm the detection of gravitational waves. The change in arm length ΔL in this situation is naturally related to the strain defined in e.q. 2.58 such that

$$h_c = \frac{\Delta L}{L}, \tag{2.59}$$

where LIGO, for example, is sensitive to a strain of $h_c \sim 10^{-21}$ which is a change in arm length of $\Delta L \sim 10^{-18}$m.

The sensitive frequency range of such interferometer is limited by their arm length, which must be comparable to the gravitational wave length to produce meaningful signals, hence this sensitive range is around 10Hz to 10kHZ. In addition, there are sources of noise that need to be reduced to identify the gravitational waves signals, such as the thermal noise, the quantum noise of device and the influence of seismic vibrations. These noises make the stochastic background difficult to be distinquished and hence the main detected sources are resolvable coalescence of astrophysical binaries.

2.3.2 Space based interferometer

The three currently proposed major next-generation space-based gravitational wave observatories, LISA [31], Taiji [32] and Tianqin [33] are to be launched in the 2030s, where LISA and Taiji follow the orbit of the Earth and Tianqin follows a geocentric orbit. Each of these observatories consists of three spacecrafts forming a equilateral triangle (e.g. the arm length between each pair of spacecrafts is 2.5 million km for LISA, 3 million km for Taiji and 0.17 million km for Taiji), each spacecraft constantly sends laser beam to the two other spacecrafts and hence they form a triangular Michelson interferometer with each side being an arm [32; 33; 34].

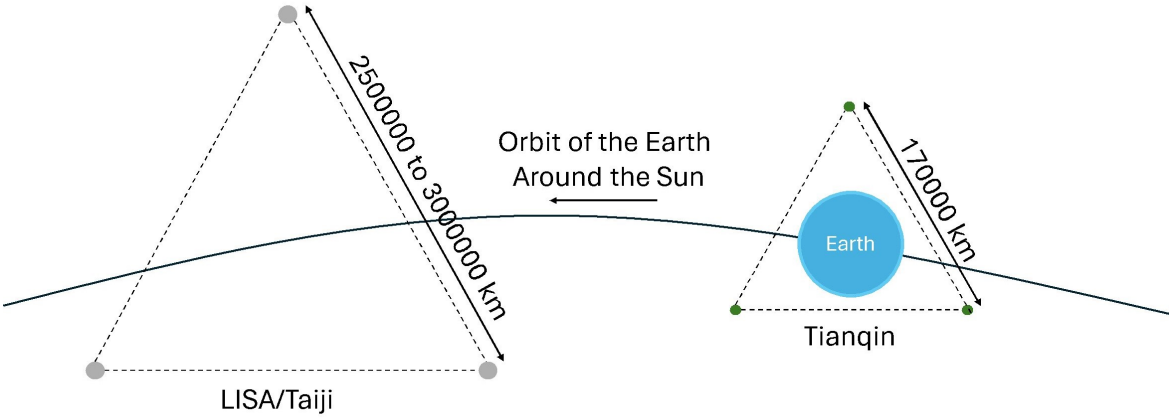

Figure 2.4: A diagrammatic illustration of the next-generation space-based gravitational wave detectors in the orbit of the Earth around the Sun. The small grey balls that follow the same orbit as the Earth represent the spacecrafts of LISA of Taiji, whereas the green ones that follow the geocentric orbit represent the spacecrafts of Tianqin.

The long arm length of these space-based interferometers makes their sensitive frequency range to be much lower, which is around 1mHz to 1Hz for LISA & Taiji and 0.1Hz to 1Hz for Tianqin, and a much higher sensitivity despite the mininal detectable strain around $h_c \sim 10^{-22} - 10^{-21}$ similar to ground-based interferometers [34].

The different instrumental designs of these observatories make their observed data complementary to the others, hence the reliability of the results would benefit from the proper coordination of these missions. For example, the cross-correlation of LISA and Taiji can avoid the assumption of having a perfect knowledge of noise statistics unlike for the individual measurements [35].

2.3.3 Pulsar timing arrays

Pulsar timing arrays, such as EPTA [36], NANOGrav [37] and PPTA [38], are observational experiments base on radiotelescopes aiming to detect very low frequency

gravitational waves of 1nHz to 1μHz by monitoring a particular set of metastable pulsars (MTPs) that should emit electromagnetic signals at a very regular time interval between two times of arrival (ToAs) [39]. This particularly low sensitive frequency range makes PTAs an unique probe to physical phenomena such as supermassive black hole binaries and other massive systems.

In reality, the propagation of MTP signals and hence their ToAs are affected by a wide range of effects, the well-known ones are the gravitational effects (e.g. Shapiro time delay) and the atmospheric effects (e.g. solar winds) [39]. The difference between the theoretical model based on these well-understood effects and the observed ToAs is referred as the residual timings. These residual timings would indicate the presence of other effects outside the theoretical model, such as the spacetime distortion induced by gravitational waves that constantly affects the propagation time of electromagnetic waves [39].

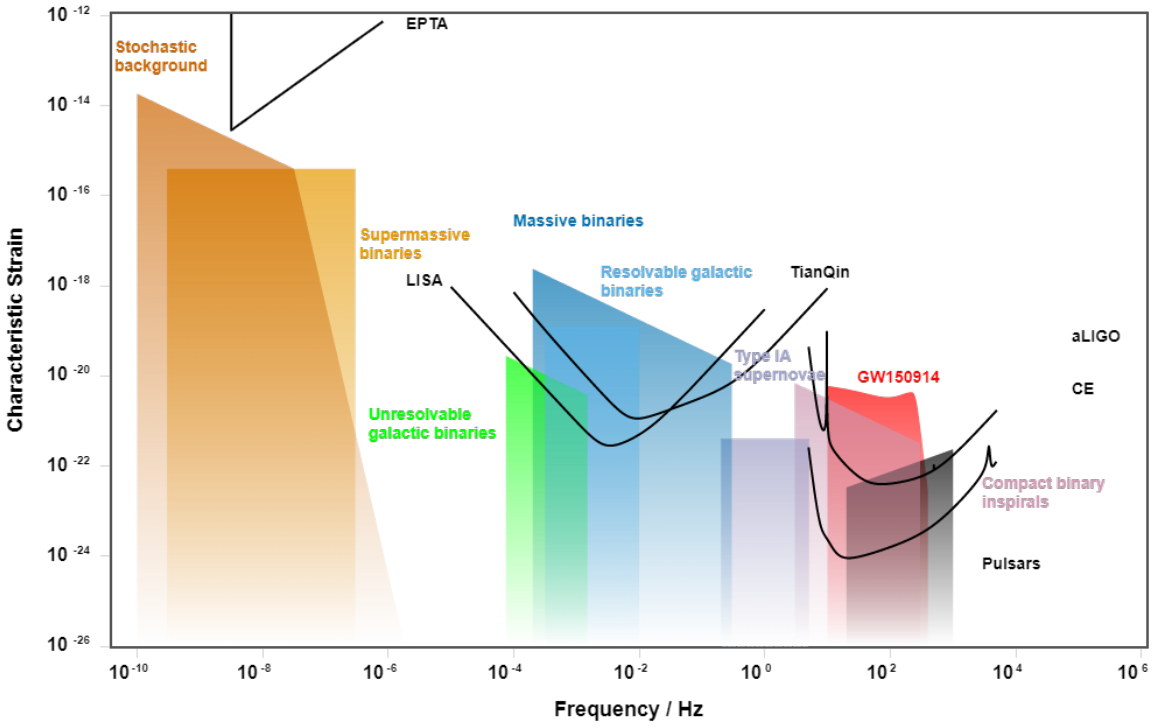

Figure 2.5: A plot of the characteristic strain against the gravitational wave frequency. The colour shaded areas are the expected characteristic strain from various sources, and the black curves represent the optimised sensitivity of some representative detectors. Plotted using gwplotter.com, credit to C. Moore, R. Cole and C. Berry.

Chapter 3

Potential sources of high-frequency gravitational waves

High-frequency gravitational waves (HFGWs) are used to describe gravitational waves with frequency above the sensitivity range of the current ground-based detectors, i.e. $f \gtrsim 10$kHz. The major current gravitational wave detectors are all designed for low frequency range ($f \lesssim 10$kHz), but before discussing the possible strategies of HFGWs detection, we should first identify the possible sources of gravitational waves. These sources can be crudely classified into two categories: the extreme processes related to (primordial) black holes or cosmological evolution, but there are a wide range of other sources that will be briefly discussed at the end of this Chapter. In this Chapter, we will give a more qualitative discussion of these sources, while paying particular attention to their detectability by considering the strain or/and energy density spectrum they could potentially produce.

3.1 HFGWs sourced by (Primordial) black holes

3.1.1 Primordial black holes merger

Unlike stellar black holes formed in late universe due to collapse of dead stars, the primordial black holes (PBHs) formed under density fluctuation in early universe can have solar or even sub-solar masses. As shown in e.q. 2.38, lower the mass of a component black hole, higher the frequency emitted by the inspiral binary, so the coalescence of PBHs could produce gravitational waves in above-MHz frequency range (much higher than the maximal frequency level $\sim 1 - 10$kHz for stellar black holes) [40].

Consider a more general binary PBH system with two black holes of masses M_1 and M_2 at a distance r from us, the characteristic strain induced by the emitted gravitational wave of frequency f is

$$h_c = 8.6 \times 10^{-22} \left(\frac{M_{\text{chirp}}}{M_S}\right)^{\frac{5}{6}} \left(\frac{f}{1\text{Mhz}}\right)^{-\frac{1}{6}} \left(\frac{r}{20\text{Mpc}}\right)^{-1}, \tag{3.1}$$

where $M_{\text{chirp}} = \frac{(M_1 M_2)^{\frac{3}{5}}}{(M_1+M_2)^{\frac{1}{5}}}$ is referred as the chirp mass of the binary system and $M_S = 2 \times 10^{10}$kg is the solar mass [41]. This strain value is within the reach of some of the currently proposed HFGW detectors, as will be discussed later in Chapter 7.

3.1.2 Primordial black hole evaporation

Black holes constantly lose energy via the Hawking radiation, i.e. the escape of one the two particles produced in the vacuum around the horizon due to quantum fluctuations. This radiation process could directly emit gravitons peaking in the frequency range of 10GHz to 1THz [40; 42], which started to occur from the formation of the PBHs and accumulates to a SGWB. The resulting energy density spectrum can be analytically computed as an integral over the proper time τ

$$\Omega_{\text{gw}}(f) = \frac{4}{\pi} \frac{\beta a_i^3 a_0^2 f^2}{H_0^2} \int_0^{\tau_f} \frac{d\tau}{a(\tau)} Q_{\text{gw}}(J, M), \tag{3.2}$$

from the start of the PBH formation $\tau = 0$ and to the PBH lifetime τ_f, where β is the fraction of PBH mass at the time of formation, Q_{gw} is the expected emission rate dependent on the angular momentum J and PBH mass M, a_i and a_0 are respectively the scales factors at the PBH formation time and the present-day [43].

In general, this energy spectrum can be contributed from either light PBHs (lighter than the critical evaporation mass $M_0 = 5 \times 10^{11}$kg) that had evaporated in the early universe before the big bang nucleosynthesis or the heavier PBHs ($M \gg M_0$) that are still evaporating today. Based on current theoretical models of PBHs, e.q. 3.2 imposes a maximal value $\Omega_{\text{gw},0}(f) \sim 10^{-7.5}$ for fully evaporated light PBHs and $\Omega_{\text{gw},0}(f) \sim 10^{-7.5}$ for evaporating heavy PBHs from Hawking radiation of PBHs [43].

3.1.3 Black hole superradiance

Superradiance is a wave amplification process when scattering off a dissipative rotating system which is a rotating black hole in this situation [44]. If massive bosons, e.g. axions (massive scalars, see Section for a proper introduction), have Compton wavelength similar to the size of black hole horizon, then they can accumulate around a rotating black hole in distinct layers to form a boson cloud, just as how electrons distribute around an atomic nucleus [44]. Any photons or gravitons emitted by the this boson cloud that scatter off the ergosphere create a superradiantly amplified signal, which could be strong enough to be directly detected.

Just as in an atom, the axions layers around the black hole is also labelled by some "quantum number" n, and the transition from a higher layer to a lower one would emit a graviton [40; 44; 45]. This transition graviton carries a frequency of

$$f = (100\text{Hz}) m_a^3 R^3 \frac{2M_S}{M}, \tag{3.3}$$

for axion mass m_a, black hole mass M and the radius of the (outer) horizon R (determined by M and the angular momentum J of the black hole) [45]. The expected strain of, e.g. the transition from the $n = 1$ layer to $n = 0$ layer is

$$h_c \sim 10^{-22} m_a^2 R^2 \left(\frac{M_{a0} M_{a1}}{M^2}\right)^{\frac{1}{2}} \left(\frac{10\text{Mpc}}{D}\right) \left(\frac{M}{2M_S}\right), \tag{3.4}$$

where M_{an} is the mass of axions in the n'th layer and D is the distance of the black hole from the detector [45].

Axions are also coupled to gravitons via high-energy physics processes: an axion pair can annihilate into a single graviton $a + a \to g$ and the produced graviton has a frequency twice of the axion Compton frequency [45]. Thus, since QCD axion is expected to have m_a between 10^{-11}eV to 10^{-10}eV (other axion-like particles can have very different masses), the expected gravitational wave frequency from this annihilation process is between 10kHz and 100kHz [46]. The upper strain limit of the induced strain is expected to be

$$h_c < 10^{-22} \left(\frac{G m_a M}{L}\right) \left(\frac{10\text{kpc}}{D}\right) \left(\frac{M}{2M_s}\right), \tag{3.5}$$

for axion (orbital) angular momentum L.

Furthermore, there is also theoretical prediction of a single axion decaying into a graviton pair ($a \to g + g$), but the frequency of the emitted photons is only half the axion Compton wavelength in this situation, the consequent strain is [40]

$$h_c < 10^{-22} \left(\frac{1\text{MHz}}{f}\right) \left(\frac{10\text{kpc}}{D}\right) \left(\frac{M}{M_s}\right)^{\frac{1}{2}}. \tag{3.6}$$

In all the three scenarios that emit superradiantly amplified gravitational waves (transition, annihilation, decay), observable strain amplitudes are expected from either massive/supermassive black holes ($M \gg M_S$) or nearby sources.

3.2 HFGWs from cosmological evolution

3.2.1 Inflation

Inflation is an accelerated exponential expansion of the universe occurred at very early times after the Big Bang, which is usually represented by a scalar field (inflaton) ϕ slowly rolling down a nearly-flat potential [47]. If existed, this expansion would rapidly stretch the quantum fluctuations in gravitational fields and hence produce an irreducible contribution to the current SGWBs which is determined by the Hubble expansion rate H during the inflation process:

$$h_0^2 \Omega_{\text{gw}}(f) \approx 5 \times 10^{-16} \left(\frac{H}{8.8 \times 10^{-13}\text{GeV}}\right)^2 \left(\frac{f}{f_{\text{CMB}}}\right)^{-\frac{1}{8}\frac{A_T}{A_S}}, \tag{3.7}$$

where $f_{\text{CMB}} \sim 10^{-18} - 10^{-17}$Hz is the CMB scale frequency, $H_0 \equiv 100h_0$km/(Mpc.s), A_T and A_S are respectively the amplitude of scalar perturbation and that of tensor perturbation with CMB imposed constraint $\frac{A_T}{A_S} \lesssim 0.1$ (e.q. 3.7 valid for inflaton-only models) [48]. However, e.q. 3.7 shows that even for mHz to Hz frequency scales, $\Omega_{\text{gw}} \sim 10^{-15}$ which is much lower than the sensitivity of any current and next-generation detectors [40].

However, it is possible to have additional contributions to Ω_{gw} from the inflation by introducing extra degrees of freedom, which can be achieved in multiples ways, such as considering modified gravity theories or introducing extra particle species produced during/after the inflation, which involve higher order perturbations [47]. Consider the concrete example of axion inflation, i.e. identify the inflaton ϕ as the axion, by introducing a coupling term between ϕ and some gauge fields $F_{\mu\nu}$ of the form

$$\mathcal{L}_{\text{int}} = \frac{\phi}{4f_a} F_{\mu\nu}\tilde{F^{\mu\nu}}, \tag{3.8}$$

where f_a is the axion decay constant and $\tilde{F}$ is the dual of F. The gauge symmetry here is usual chosen to be U(1) to ensure radiative stability which requires parameters used in an inflation model to be stable after introducing quantum correction [48]. The existence of the coupling term e.q. 3.8 induced a source term in the corresponding Einstein equations, then by following the similar approach as in Section 2.2, we obtain

$$\Omega_{\text{gw}} \sim 2.3 \times 10^{-7} \Omega_{\text{rad}} \frac{f_a^6 H^{10}}{G^2 \dot{\phi}^6} e^{\frac{2\pi\dot{\phi}}{f_a H}}, \tag{3.9}$$

where Ω_{rad} is the present-day radiation density [40]. Although higher $\dot{\phi}$ would significantly increase the energy density of SGWB at present-day, but the slow-roll condition imposes that $\dot{\phi} < 10 f_a H$, and hence we expect a maximal density of $\Omega_{\text{gw}} \sim 10^{-10}$ from the axion inflation [40].
It is also worth mentioning that the PBHs would be formed as a consequence of inflation when the quantum fluctuations reenter the horizon, but their impacts on SGWBs have been discussed previously.

3.2.2 (P)reheating

The inflation ends when the slow-rolling inflaton field ϕ reaches the minimum of its potential and then oscillates around the latter, which releases a huge amount of energy in the form of various elementary particles that interact with each other to eventually reach the thermal equilibrium [49]. Since the temperature of the universe significantly dropped down after inflation, the release of these particles increases the temperature again and hence this process is referred as reheating [47; 49].

However, reheating is taken to be a perturbative process since the oscillation of the inflaton field ϕ is expected to be small, but if ϕ is coupled to some matter field (either fermion or boson), the particle production via oscillation can be exponentially amplified to cause the parametric resonance instability that needs to be treated

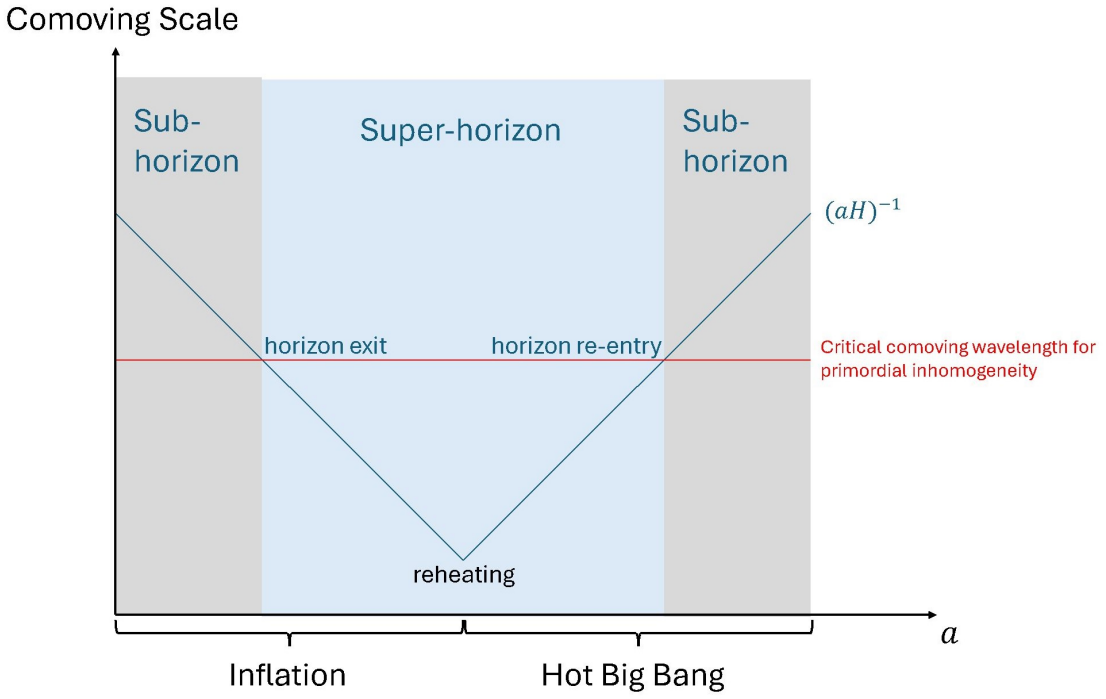

Figure 3.1: A plot illustrating the change in the comoving scale of primordial inhomogeneities in the early universe. The inflation makes the causally connected inhomogeneities out of each other's horizon, which explains the horizon problem in cosmology. After reheating, the comoving scale increases again and eventually re-enter the horizon, at which point the primordial black holes could form if the inhomogeneities were dense enough.

non-perturbatively [40; 47; 50]. We refer this instability as preheating as an intermediate process between the end of inflation and reheating, which occurs when ϕ has an energy density much stronger than that of matter fields and ends when these two energy densities are comparable [47].

The parametric resonance amplifies the energy density of matter fields in some specific resonance bands, which causes inhomogeneities in the energy density of the universe. These inhomogeneities are time-dependent and hence induce rapid changes in quadruple moment to produce a large amount of primordial gravitational waves. From the end of inflation $t = t_i$ to the reach of reheating-induced thermal equilibrium t_*, the coefficient ω_{EoS} of the equation of state rapidly jumps from $\omega_{\text{EoS}} = 0$ to $\omega_{\text{EoS}} = \frac{1}{3}$ during preheating at $t = t_j$, with a mean value $\bar{\omega}$ depending on the details of a specific inflation/reheating model [47; 51]. By considering the change in scale factor of the universe during (p)reheating, the frequency of gravitational waves at present-day due to these inhomogeneities can be estimated via

$$f \approx \frac{k}{a_j \rho_j^{\frac{1}{4}}} \left(\frac{a_j}{a_*}\right)^{1-\frac{3(1+\bar{\omega})}{4}} 4 \times 10^{10}\text{Hz}, \tag{3.10}$$

where a_j and ρ_j are respectively the scale factor and total energy density at $t = t_j$, a_* is the scale factor at t_* and k is the comoving wave-number [51]. The corresponding SGWBs spectrum is

$$\Omega_{\text{gw}} = \frac{S_f(\eta_f)}{a_j^4 \rho_j} \left(\frac{a_j}{a_*}\right)^{1-3\bar{\omega}} \Omega_{\text{rad}}, \tag{3.11}$$

where the scale factor modulated gravitational wave spectrum S_f is defined to be

$$S_f(\eta_f) = a^4(\eta) \left(\frac{d\rho_{\text{gw}}}{d\ln f}(\eta > \eta_f)\right), \tag{3.12}$$

for conformal time $\eta = \eta_f$ where the oscillation of inflaton becomes a negligible source to gravitational wave [51].

3.2.3 Phase Transitions

In cosmology, phase transitions are thought as the transition from one vacuum ground state to another, which are usually related to the symmetry breaking processes occurred in the early universe, such as the breaking of the electroweak symmetry [52]. Phase transitions are categorised into the first order phase transition and the second order order transition, where the second order transitions correspond to continuous evolution of the ground state [52]. On the other hand, the first order phase transitions refer to discontinuous change in the vacuum ground state, which is usually modelled by the nucleation of bubbles filled by the new lower-temperature phase due to quantum fluctuations, these bubbles expand in the old stable background phase and would eventually occupy the entire universe to form the new background phase to complete the phase transition [52; 53].

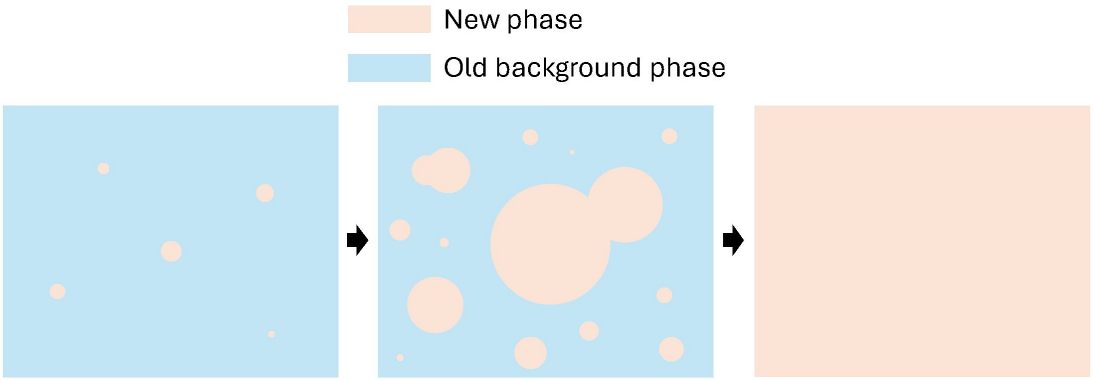

Figure 3.2: A plot illustrating the 1st order phase transition occurred in the early universe. Bubbles of the new phase (light orange) randomly appear due to quantum fluctuations in the universe which is in the old background phase (light blue) (left). These bubbles expand to some extend that they collide and merge with the others (middle), during which a large amount of gravitational waves is emitted. Finally, the new phase replaces the old one as the bubbles occupy the entire universe (right).

The bubbles expand in hot plasma and would collide with each other when they are large enough, this collision process would release a huge amount of latent heat since the energy of the bubbles is stored in their walls [52; 53]. The primary gravitational waves from the collision of these bubbles are due to the deformation of the spherical structure of the bubble walls, but the collision events also disturb the surrounding plasma in the form of sound waves (i.e. periodic acoustic compression of plasma) and turbulent shock waves, which also release gravitational waves [40; 53].

The resulting energy density spectrum from the gravitational waves receives contributions from these three factors, bubble wall deformation, sound waves and turbulence, which are the first, second and third terms in the square bracket of the following expression obtained by making the envelope approximation (i.e. the gravitational waves produced only depend on the shape of part of the bubble wall not in contact with other bubble walls) via

$$\begin{aligned} h^2\Omega_{\text{gw}}(f) = v_w H \left(\frac{\Gamma}{\dot{\Gamma}}\right) \left(\frac{\rho_{\text{vac}}}{\rho_{\text{rad}}+\rho_{\text{vac}}}\right)^2 \left(\frac{100}{g}\right)^{\frac{1}{3}} \\ \times \left[1.84\times10^{-6}\kappa \left(\frac{v_w^2}{0.42+v_w^2}\right) S_{\text{env}}(f) + 2.65\times10^{-6}\kappa_v S_{\text{sw}}(f) \right. \\ \left. + 3.35\times10^{-4}\kappa_{\text{turb}}^{\frac{3}{2}} \left(\frac{\rho_{\text{rad}}+\rho_{\text{vac}}}{\rho_{\text{vac}}}\right)^{\frac{1}{2}} S_{\text{turb}}(f)\right], \end{aligned} \tag{3.13}$$

where ρ_{vac} and ρ_{rad} are vacuum and radiation densities, Γ is the bubble nucleation rate, v_w is the velocity of bubble wall expansion, κ_v is the fraction vacuum energy turned into the kinetic energy of the plasma, κ and κ_{turb} are respectively the fractions of the latent heat stored in the bubble walls and converted into turbulent kinetic energy, all these quantities are measure at the time of nucleation [54]. The frequency dependent spectral shapes $S_{\text{env}}(f)$, $S_{\text{sw}}(f)$ and $S_{\text{turb}}(f)$ heavily depend on the temperature at which the nucleation of bubbles happened, and the resulting peaking frequency of the spectrum e.q. 3.13 from numerical simulations is around 1MeV to 1TeV at present-day [40].

3.3 A brief discussion of other possible sources

The sources of HFGWs listed above are the majors ones that we expect from both the Standard model of particle physics and that of cosmology (namely the LCDM model), except for a couple of specific examples related to axions. However, there is a range of other possible sources closely related to the ones above but they usually assume high energy theories beyond the Standard Model (BSM) of particle physics. A classe of examples of such sources is compact objects made of exotic particles, such as axions and supersymmetric particles like gravitinos (fermionic supersymmetric partner of graviton) [40].

Another important classe of HFGWs sources is based on the Grand Unified Theories (GUTs) such as the (super)string theory, where cosmic topological defects are

formed during phases transitions and carry information about the broken symmetries [55]. For example, the breaking of a continuous symmetry would lead to the formation of cosmic strings and/or magnetic monopoles if the vacuum manifold had appropriate topological properties (e.g. not being simply connected), whereas the breaking of a discrete symmetry could lead to the formation of domain walls (regions with distinct vacua) [56; 57]. Another example is the higher-dimension scenarios like brane-world cosmology that appear in supersymmetry and modified gravity (such as the Dvali-Gabadadze-Porrati model), where our universe is described a 4-dimensional brane embedded in a higher-dimensional bulk and the intersections of different branes could be regarded as a form of topological defects [58]. The motions or/and vibrations of these topological defects should in principle lead to observable perturbation to the spacetime of the universe and hence produce gravitational waves at a large frequency range of gravitational waves, hence gravitational waves (especially HFGWs) are an unique probe to these high energy theories far beyond the reach of the current particle colliders such as the LHC at CERN.

Chapter 4

An up-to-date formalism of the (inverse) Gertsenshtein effect

Despite being first derived by Boccaletti and Zel'dovich in 70s [7; 8], Dyson proposed a simpler and more up-to-date derivation of the (inverse) Gertsenshtein effect, as presented in [59]. However, as pointed out very recently in [60], one must keep in mind that this Dyson's derivation simplifies the treatment of electric and magnetic fields by ignoring the contribution from the metric [60; 61]. Thus, the results obtained from this derivation is only correct for a constant background magnetic field. Nonetheless, this simplification has been assumed in most of the existing literature and many scenarios we study can indeed be approximated as having constant background magnetic field at suitable scales. Hence we will adopt this derivation for the moment by completing intermediate steps missing in the existing literature, with a brief discussion of the complete treatment at the end of this chapter.

4.1 Gravity-electromagnetism coupling

As mentioned in section 2.1, we work in linearised gravity with metric

$$g_{\mu\nu} = \eta_{\mu\nu} + h_{\mu\nu}, \tag{4.1}$$

and work in the transverse-traceless (TT) gauge that constraints this perturbation such that [60; 62]

$$h^{\mu}_{\mu} = h_{0i} = \partial_j h_{ij} = 0, \tag{4.2}$$

and the GWs have two polarisations h_+ and $h_\times$ such that

$$h_{ij} = \begin{pmatrix} h_+ & h_\times & 0 \\ h_\times & -h_+ & 0 \\ 0 & 0 & 0 \end{pmatrix}. \tag{4.3}$$

To the linear approximation, the action for a system with both gravitational and electromagnetic fields can be written as

$$S = S_{\text{EH}} + S_{\text{EM}}. \tag{4.4}$$

The two terms on the right-hand side are the Einstein-Hilbert action and the action with a minimal coupling between electromagnetic and gravitational fields, respectively [3; 11]. If neglecting the back-reaction effects on the GWs [59; 62]

$$S_{\rm EH} = \frac{1}{16\pi G}\int d^4x\sqrt{-g}R; \tag{4.5}$$

$$S_{\rm EM} = -\frac{1}{4}\int d^4x\sqrt{-g}g^{\mu\alpha}g^{\nu\beta}F_{\mu\nu}F_{\alpha\beta}, \tag{4.6}$$

where $g = \det(g_{\mu\nu})$, G is the Newton's gravitational constant, R is the Ricci scalar, $F_{\mu\nu} = \partial_\mu A_\nu - \partial_\nu A_\mu$ with vector potential A_μ is the Maxwell strength tensor.

4.2 Photon-graviton conversion (inverse process)

By noting that $g = 1 + O(h_{ij}^2)$, the following vacuum Einstein-Maxwell equations can be readily obtained [59; 60] by variating e.q. 4.4:

$$(g^{\mu\alpha}g^{\nu\beta}F_{\alpha\beta})_{,\nu} = ((\eta^{\mu\alpha} - h^{\mu\alpha})(\eta^{\nu\beta} - h^{\nu\beta})F_{\alpha\beta})_{,\nu} = 0, \tag{4.7}$$

keep to the linear order and choose $\mu = i$, this becomes

$$F_{ij,j} + F_{i0,0} - (h^{ij}F_{ij})_{,k} - (h^{ij}F_{0j})_{,0} = 0, \tag{4.8}$$

where we have used e.q. 4.2 and symmetric (antisymmetric) properties of $F_{\mu\nu}$ and h_{ij}. Now take the electric and magnetic fields ignoring the metric contributions: $F_{0i} = -E_i$ & $F_{ij} = \epsilon_{ijk}B^k$, and multiply e.q. 4.8 by ϵ_{npi} [59]:

$$-\epsilon_{npi}\epsilon_{ijk}B_{k,jp} + \epsilon_{npi}E_{i,0p} - \epsilon_{npi}\epsilon_{jkl}(B^l h^{ij})_{kp} - \epsilon_{npi}(h^{ij}E_j)_{,0p} = 0, \tag{4.9}$$

and use $\nabla\times(\nabla\times\boldsymbol{B}) = -\nabla^2\boldsymbol{B} = -\boldsymbol{B}''$ and $\nabla\times\boldsymbol{E} = -\dot{\boldsymbol{B}}$, we obtain

$$(\partial_0^2 - \nabla^2)B_i = \nabla^2(h_{ij}B^j) - \nabla_i(h^{ij}B_{j,k}). \tag{4.10}$$

Consider a uniform background magnetic field $\boldsymbol{B}_0$ with a small induced magnetic field $\boldsymbol{b}$ such that $\boldsymbol{B} = \boldsymbol{B}_0 + \boldsymbol{b}$ and $|\boldsymbol{b}| \ll |\boldsymbol{B}_0|$, e.q. 4.10 can be expressed as [59; 60]

$$(\partial_0^2 - \nabla^2)b_i = -\Box b_i = \nabla^2 h_{ij}B_0^j, \tag{4.11}$$

where we employed the condition in TT gauge $(\partial_0^2 - \nabla^2)(h_{ij}B^j) = 0$ and work in the linear order of smallness [60]. Hence it can be learnt from e.q. 4.11 that the existence of a background magnetic field is necessary for graviton-photon conversion [59]. If the incident gravitational wave is in the z-direction, then the components of the above wave equation are [60]

$$-\Box b_1 = h_{+,zz}B_0^{(1)} + h_{\times,zz}B_0^{(2)}, \tag{4.12}$$

$$-\Box b_2 = h_{\times,zz}B_0^{(1)} - h_{+,zz}B_0^{(2)}, \tag{4.13}$$

$$-\Box b_3 = 0, \tag{4.14}$$

from which we see that the generated electromagnetic waves are orthogonal to the incident GWs [59] (where (i) is used to denote components of $\boldsymbol{B_0}$ to avoid confusion).
Although it is phenomenologically more favorable to only employ the physical quantities E_i and B_i, working with the vector potential A_μ is a common practice in existing literature. The use of vector potential avoids the problem of metric dependency of E_i and B_i in curved spacetime as mentioned previously, but converting A_μ into E_i and B_i is still metric dependent in general [60], which will also be discussed in the following section. In our simplified discussion without metric dependency, $B_i = \epsilon_{ijk}\partial_j A_k$, and e.q. 4.11 turns into

$$-\epsilon_{ijk}\Box A_{k,j} = \nabla^2 h_{ij} B_0^j, \tag{4.15}$$

and hence

$$\Box A_1 = -h_{\times,z} B_0^{(1)} + h_{+,z} B_0^{(2)}, \tag{4.16}$$

$$\Box A_2 = h_{+,z} B_0^{(1)} + h_{\times,z} B_0^{(2)}, \tag{4.17}$$

$$\Box A_3 = 0. \tag{4.18}$$

4.3 Graviton-Photon conversion

The differential equations governing graviton-photon conversion can be directly derived from e.q. 2.13, where on the left-hand side the stress tensor T_{ij} due to electric and magnetic fields E and B takes the form

$$\begin{aligned} T_{ij} &= E_i E_j + B_i B_j - \frac{1}{2}\delta_{ij}(E_k^2 + B_k^2) \\ &= B_0^{(i)} B_0^{(j)} + b_i B_0^{(j)} + b_j B_0^{(i)} - \frac{1}{2}\delta_{ij}((B_0^{(k)})^2 + 2B_0^{(k)} b_k), \end{aligned} \tag{4.19}$$

where for the last step we used assumptions $\boldsymbol{B} = \boldsymbol{B}_0 + \boldsymbol{b}$ and $|\boldsymbol{b}| \ll |\boldsymbol{B}_0|$ previously mentioned, as well as $|\boldsymbol{E}| \ll |\boldsymbol{B}_0|$ and that the incident waves propagate in z-direction.
Therefore, the components of e.q. 2.13 are

$$\Box h_{11} = -\Box h_{22} = -16\pi G(\frac{1}{2}(B_0^{(1)})^2 - \frac{1}{2}(B_0^{(2)})^2 + B_0^{(1)} b_1 - B_0^{(2)} b_2), \tag{4.20}$$

$$\Box h_{12} = \Box h_{21} = -16\pi G(B_0^{(1)} B_0^{(2)} + B_0^{(2)} b_1 + B_0^{(1)} b_2), \tag{4.21}$$

$$\Box h_{i3} = \Box h_{3i} = 0. \tag{4.22}$$

We can reform e.q. 4.20 and e.q. 4.21 in terms of vector potential A_i as done previously

$$\Box h_{11} = -\Box h_{22} = 16\pi G(B_0^{(1)} \partial_z A_2 + B_0^{(2)} \partial_z A_1), \tag{4.23}$$

$$\Box h_{12} = \Box h_{21} = 16\pi G(B_0^{(2)} \partial_z A_1 - B_0^{(1)} \partial_z A_2), \tag{4.24}$$

where the constant terms in e.q. 4.20 and e.q. 4.21 can be removed by field redefinition/appropriate transformation.

4.4 Complication due to electromagnetism in curved spacetime

The above derivation implicitly assumes that the components of the Maxwell field strength tensor $F_{\mu\nu}$ in curved spacetime adopt the same forms as in special relativity for flat Minkowski spacetime, which is also the assumption in most current literature. However, it has been recently pointed out that such assumption is physically not valid due to the impossibility of choosing a proper observer, which may only be solved by introducing the metric into the components of $F_{\mu\nu}$ [60; 61].

Consider an observer moving with an arbitrary timelike four-velocity u_μ, then there is always a covariant decomposition of $F_{\mu\nu}$ which defines the electric and magnetic field vectors covariantly by choosing a particular u_μ:

$$F_{\mu\nu} = u_\mu E_\nu - u_\nu E_\mu - \eta_{\mu\nu\alpha\beta} u^\alpha B^\beta, \tag{4.25}$$

where the 4-index Levi-Civita tensor and the 3-index Levi-Civita symbol are related by $\eta_{0ijk} = -\sqrt{-g}\epsilon_{ijk}$ [63]. If choosing $u_\mu = (-1, 0, 0, 0)$ and $\sqrt{-g} = 1$, then the usual expression for components of $F_{\mu\nu}$ are directly recovered just as in special relativity. However in curved spacetime, this is not true since in general $\sqrt{-g} \neq 1$ and the choice of $u_\mu = (-1, 0, 0, 0)$ would leave

$$F_{0i} = -E_i,\ F_{ij} = \sqrt{-g}\epsilon_{ijk} B^k \tag{4.26}$$

and there is no other choice to simultaneously recover all the relations in special relativity [61]. This means that no observer can in general see the electric and magnetic fields if being related to $F_{\mu\nu}$ as in Minkowski spacetime, which can also used to show that the physical observables like the charge and current densities cannot be properly defined [61].

In the normal frame, the components of $F_{\mu\nu}$ can be covariantly chosen to be

$$F_{0i} = -E_i,\ F_{ij} = \epsilon_{ijk}(B^k - h^{kl} B_k), \tag{4.27}$$

and, consequently, the Maxwell equations that involve derivatives of B_i take the form [60]

$$\partial_i B^i = \partial_i (h^{ij} B_j), \tag{4.28}$$

$$\partial_0 B^i + \epsilon^{ijk} \nabla_i E_k = \partial_0 (h^{ij} B_j). \tag{4.29}$$

Consider again the scenario in the previous parts of this chapter by splitting the total magnetic field into the background contribution and the induced contribution, the above Maxwell equations give

$$(\partial_0^2 - \nabla^2) b_i = \partial_0^2 (h_i^j B_j) - \nabla_i (h_{jk} \partial_k B_j), \tag{4.30}$$

which coincides to be the same as e.q. 4.11 for constant background magnetic field $\boldsymbol{B} = \boldsymbol{B}_0$ [60].

Chapter 5

Cosmological implications of the Gertsenshtein effect

As will be shown in concrete examples, the graviton to photon conversion rate due to the inverse Gertsenshtein effect is highly suppressed, and hence one needs to consider extreme settings that could create detectable photon signals. One possibility is to consider background magnetic field at galactic or cosmic scales to compensate weak conversion rate [64]. But for this purpose, we need to consider the plasma and other effects that are important in actual astrophysical/cosmological scenarios.

5.1 Presence of plasma and QED correction

In the formalism of Chapter 3, we considered a toy model consisting of a background magnetic field in the vacuum. However, in actual astrophysical/cosmological scenarios, one also has to consider how the presence of medium affects the propagation of photons in this background magnetic field. The wavelength k and the (angular) frequency ω of electromagnetic waves obey the dispersion relation $k = n\omega$ for some refractive index n which deviates from 1 due to the presence of any medium other than vacuum. Therefore, the photons acquire an effective mass $m_\gamma = \omega^2 - k^2 = (1-n^2)\omega \neq 0$ when propagating through the medium. For the astrophysical/cosmological scenarios we are interested in, the dominant medium to be considered is plasma, i.e. free electrons. However, an accurate description of the physics beyond the classical level requires the consideration of multiple factors.

Plasma

Free electrons permeate the entire universe at all scales (in intercluster medium, intergalactic medium, interstellar medium etc) and have various origins such as reionisation, radiations from compact objects, supernovae etc.
The classical impacts of plasma on the propagation of photons can be incorporated by introducing an additional source term into the electromagnetic part of the action

e.q. 4.6:

$$S_{\text{EM,pl}} = -\int d^4x\sqrt{-g}g^{\mu\nu}j_\mu A_\nu. \tag{5.1}$$

To construct the form of j^μ, consider a general electromagnetic current induced by free electrons with momentum p^i, $j^i = e\frac{n_e p^i}{m_e}$, for electron charge e, electron density n_e and electron mass m_e. Lorentz force law with relativistic corrections approximates to $p^i = -eA^i$ [65], hence

$$j^\mu = -\omega_{pl}^2 A^\mu \tag{5.2}$$

where the characteristic plasma frequency is $\omega_{pl} = \sqrt{e\frac{n_e}{m_e}}$. Thus, the presence of plasma modifies the refractive index as

$$\Delta n_{\text{plasma}} = \sqrt{1 - \frac{\omega_{pl}^2}{\omega^2}} - 1 \approx -\frac{\omega_{pl}^2}{2\omega^2}, \tag{5.3}$$

where the propagation is only possible if $\omega > \omega_{pl}$ the second approximated equality holds for small plasma frequency (usually meaning low plasma density).

QED correction

However, the propagation of photons is influenced by the vacuum polarisations: the temporary conversion of photons into electron-position pairs. In the language of quantum field theory, this is just the one-loop correction to the free photon propagator, represented by the following Feynman diagram:
In general, to introduce this QED correction to our theory, the following non-linear component, the Heisenberg-Euler action, is added to the action

$$S_{\text{QED}} = -\frac{1}{2}\int d^4x \int d^4x' A_\mu(x)\Pi^{\mu\nu}A_\mu(x'), \tag{5.4}$$

where $\Pi^{\mu\nu}$ is the photon self-energy [62; 66; 67]. It is worth noting that for this analysis of the (inverse) Gertsenshtein mechanism, we are only considering the interaction between photons, so we are neglecting the interaction term $-e\bar{\Psi}\gamma^\mu\Psi A_\mu$ that contains antispinor/spinor $\bar{\Psi}/\Psi$ (electron/positron). However, this is only valid up to $1\text{MeV} \sim 2m_e \sim 10^{21}\text{Hz}$ frequency scale, since beyond which the photons are energetic enough to be converted into electron-positron pairs and hence the assumption breaks down [68]. Much lower than this frequency bound $\omega \sim 100\text{TeV}$, the effective QED correction e.q. 5.4 reduces to

$$S_{\text{QED,eff}} = \frac{\alpha^2}{90m_e^4}\int d^4x\sqrt{-g}[(F_{\mu\nu}F^{\mu\nu})^2 + \frac{7}{4}(\tilde{F}_{\mu\nu}F^{\mu\nu})^2], \tag{5.5}$$

where $\alpha = \frac{e^2}{4\pi}$ is the fine structure constant for electron charge e and $\tilde{F}_{\mu\nu} = \epsilon_{\mu\nu\alpha\beta}F^{\alpha\beta}$ is the dual to $F_{\mu\nu}$ [66; 69; 70]. This vacuum polarisation should, in principle, contribute to the total refractive index by an amount Δn_{QED}. This contribution is determined by the a characteristic magnetic field $B_c = \frac{m_e^2}{e} \approx 4.41 \times 10^{13}G$ of the Heisenberg-Euler action

$$\Delta n_{\text{QED}} = \frac{\alpha}{45\pi}\left(\frac{B_0}{B_c}\right)^2, \tag{5.6}$$

hence this contribution is usually suppressed due to the large value of B_c [11; 71].

Cotton-Mouton effect

By splitting $F_{\mu\nu}$ into the constant part $F_{(0)\mu\nu}$ (constant external field with $|\boldsymbol{B}| \gg |\boldsymbol{E}|$) and the propagating part $f_{\mu\nu}$ (incident wave), the system manifests the birefrigence effects, i.e. different refractive indeces along different directions [11; 72]. Inserting $F_{\mu\nu} = F_{(0)\mu\nu} + f_{\mu\nu}$ into the action of electromagnetism with non-linear contribution e.q. 5.5 and work with the resulting modified Maxwell's equations, the following refractive indices for different polarisations are obtained:

$$n_+^2 = 1 + 4\rho B_0^2 \sin^2\phi \tag{5.7}$$

$$n_\times^2 = 1 + 7\rho B_0^2 \sin^2\phi \tag{5.8}$$

where n_+ denotes the polarisation transverse to the polarisation of B_0, $n_\times$ denotes the polarisation parallel to the polarisation of B_0 and ϕ is the angle between the direction of B_0 and the incident electromagnetic wave [11; 71].
For small B_0, e.q. 5.9 and e.q. 5.10 reduce to

$$n_+ = 1 + 2\rho B_0^2 \sin^2\phi \tag{5.9}$$

$$n_\times = 1 + \frac{7}{2}\rho B_0^2 \sin^2\phi. \tag{5.10}$$

Therefore, the difference between the two refractive indices $\Delta n = |n_+ - n_\times|$ is proportional to the square of the external magnetic field, which is exactly the birefringence behaviour expected from the Cotton-Mouton effect [11; 66; 71]. Physically, the appearance of this birefringence effect is due to the external magnetic field pointing in some particular direction, which destroys the overall isotropy of the plasma hence the photons would propagate differently along difference directions [11; 73]. Hence the total refractive indeces for $+$ and $\times$ polarisations are

$$n_{+,\times} = 1 + \Delta n_{\text{plasma}} + \Delta n_{\text{QED}} + \Delta n_{\text{CM};+,\times}. \tag{5.11}$$

Scattering with CMB photons

The photons produced by gravitons via the inverse Gertsenshtein mechanism can contribute to the total refractive index by an amount

$$\Delta n_{\text{CMB}} = \frac{88\pi^2\alpha^2 T_0^4 \omega}{2025 m_e^2}, \tag{5.12}$$

which is proportional to ω and hence only become significant for frequency above $\sim 10^{23}$Hz [74]. This frequency limit is much higher than the upper frequency bound placed by the effective QED theory e.q. 5.5 as discussed previously, hence this contribution is not taken into account in the our analysis.

5.2 Gertsenshtein mechanism in WKB approximation

Consider again a electromagnetic wave propagating in z-direction and enters a region with constant background magnetic field of strengh B_0. For mathematical convenience that will become evident soon, we redefine $h_{\mu\nu} \to \frac{1}{\kappa}h_{\mu\nu}$ for $\kappa = \sqrt{16\pi G}$ and hence $g_{\mu\nu} \to g_{\mu\nu} = \eta_{\mu\nu} + \kappa h_{\mu\nu}$ [11; 72]. The modification of the refractive index due to plasma, vacuum polarisation and Cotton-Mouton effect alter the differential equations e.q. 4.16 and e.q. 4.17

$$(\Box - m_\gamma^2)A_1 = \kappa h_{+,z} B_0^{(2)}, \tag{5.13}$$

$$(\Box - m_\gamma^2)A_2 = \kappa h_{\times,z} B_0^{(2)}, \tag{5.14}$$

where we performed a rotational transformation in the x-y plane which is transverse to the direction of propagation so that $\boldsymbol{B}_0 = (0, B_0, 0)^T$ [11; 72]. On the other hand, e.q. 4.23 and e.q. 4.24 are not affected since there is no effective mass for graviton:

$$\Box h_{11} = -\Box h_{22} = \kappa B_0^{(2)} \partial_z A_1, \tag{5.15}$$

$$\Box h_{12} = \Box h_{21} = \kappa B_0^{(2)} \partial_z A_1. \tag{5.16}$$

Now expand both $h_{ij}(t, \boldsymbol{x})$ and $A_i(t, \boldsymbol{x})$ in their polarisation bases $\hat{\boldsymbol{e}}_{ij}^{\lambda}$ and $\hat{\boldsymbol{e}}_i^{\lambda}$ (no Fourier transform performed unlike in e.q. 2.47):

$$h_{ij}(t, \boldsymbol{x}) = \sum_{\lambda=+,\times} h_\lambda(\boldsymbol{x}) \hat{\boldsymbol{e}}_{ij}^{\lambda} e^{-i\omega t}, \tag{5.17}$$

$$A_i(t, \boldsymbol{x}) = \sum_{\lambda=+,\times} A_\lambda(\boldsymbol{x}) \hat{\boldsymbol{e}}_{i}^{\lambda} e^{-i\omega t}, \tag{5.18}$$

where the components of the vector potential are identified by polarisation index λ such that $A_+ = A_1$ and $A_\times = A_2$ [11; 72; 73]. Using these expansions, e.q. 5.13, e.q. 5.14, e.q. 5.15 and e.q. 5.16 can be rearranged in terms of the polarisation index λ

$$(\omega^2 + \partial_z^2)A_\lambda + (k^2 - \omega^2)A_\lambda = -i\kappa(\partial_z h_\lambda)B_0, \tag{5.19}$$

$$(\omega^2 + \partial_z^2)h_\lambda = -i\kappa \partial_z A_\lambda B_0. \tag{5.20}$$

Although the exact solutions to these second order differential equations exist (see [62]), the full derivation of the exact solutions is very lengthy and complicated. In most literature, these differential equations are simplified to first order differential equations using the WKB approxition: assume that the wavelength of photons is much lower than the coherence wavelength of B_0 and the modification to the refractive index due to the previously mentioned factors is very small $|n - 1| \ll 1$ [11; 71; 72], then

$$\omega^2 + \partial_z^2 = (\omega + i\partial_z)(\omega - i\partial_z) \approx 2\omega(\omega - i\partial_z), \tag{5.21}$$

where we set $k = -i\partial_z$ and used $\omega + k \approx 2k$. Then e.q. 5.19 and e.q. 5.20 become

$$(\omega + i\partial_z)A_\lambda + (n-1)A_\lambda = -\frac{\kappa}{2} h_\lambda B_0, \tag{5.22}$$

$$(\omega + i\partial_z)h_\lambda = -\frac{\kappa}{2}A_\lambda B_0. \tag{5.23}$$

This set of equations can be rearranged into a concise matrix equation by defining the vector $\boldsymbol{\psi}_\lambda(z) \equiv (A_\lambda(z), h_\lambda(z))^T$:

$$\left((\omega + i\partial_z) + \begin{pmatrix} M_+ & 0 \\ 0 & M_\times \end{pmatrix}\right)\begin{pmatrix} \boldsymbol{\psi}_+(z) \\ \boldsymbol{\psi}_\times(z) \end{pmatrix} = 0, \tag{5.24}$$

where the two sub-matrices on the diagonal of the full mixing matrix take the form

$$M_\lambda = \begin{pmatrix} \Delta_\lambda & \Delta_{g\gamma} \\ \Delta_{g\gamma} & 0 \end{pmatrix}, \tag{5.25}$$

for the effective polarisation-dependent photon mass $\Delta_\lambda = (n_\lambda - 1)\omega$ and the graviton-photon coupling $\Delta_{g\gamma} = \kappa B_0$ [11; 71; 72]. Therefore the decoupled differential equations for each of the two polarisations are

$$i\partial_z \boldsymbol{\psi}_\lambda(z) + (\omega \mathbf{1} + M_\lambda)\boldsymbol{\psi}_\lambda(z) = 0. \tag{5.26}$$

To solve e.q. 5.26, one needs to first diagonalise [11; 72; 74] M_λ by performing a SU(2) transformation of the standard form

$$M_\lambda \to \tilde{M}_\lambda = SM_\lambda S^{-1}, \boldsymbol{\psi}_\lambda(z) \to \tilde{\boldsymbol{\psi}}_\lambda(z) = S\boldsymbol{\psi}_\lambda(z) \text{ for } S = \begin{pmatrix} \cos\theta & \sin\theta \\ -\sin\theta & \cos\theta \end{pmatrix}, \tag{5.27}$$

where the specific θ, referred as graviton-photon mixing angle [67; 71], that makes the off-diagonal elements of $SM_\lambda S^{-1}$ to vanish is

$$\begin{aligned} -\cos\theta\sin\theta\Delta_\lambda + (\cos^2\theta - \sin^2\theta)\Delta_{g\gamma} &= 0 \\ \Rightarrow -\frac{\sin 2\theta}{2}\Delta_\lambda + \cos 2\theta\Delta_{g\gamma} &= 0 \\ \Rightarrow \tan 2\theta &= \frac{2\Delta_{g\gamma}}{\Delta_\lambda}. \end{aligned} \tag{5.28}$$

The transformed matrix now takes the form $\tilde{M}_\lambda = \text{diag}(\Delta_1^\lambda, \Delta_2^\lambda)$ where

$$\Delta_{1,2}^\lambda = \frac{\Delta_\lambda}{2} \pm \sqrt{\frac{\Delta_\lambda^2}{4} + \Delta_{g\gamma}^2} \tag{5.29}$$

are the eigenvalues of M_λ. Thus, the formal general solutions to $\boldsymbol{\psi}$ and hence $\tilde{\boldsymbol{\psi}}$ are

$$\tilde{\boldsymbol{\psi}}(z) = e^{i\int_0^z(\omega+\tilde{M})dz'}\tilde{\boldsymbol{\psi}}(0) \tag{5.30}$$

$$\Rightarrow \boldsymbol{\psi}(z) = e^{i\omega z}e^{i\int_0^z S^{-1}MSdz'}\tilde{\boldsymbol{\psi}}(0), \tag{5.31}$$

which can be explicitly written out in terms of individual components

$$A_\lambda(z) = J_\lambda(z; \cos^2\theta, \sin^2\theta)A_\lambda(0) + J_\lambda(z; \sin\theta\cos\theta, -\sin\theta\cos\theta)h_\lambda(0), \tag{5.32}$$

$$H_\lambda(z) = J_\lambda(z; \sin\theta\cos\theta, -\sin\theta\cos\theta)A_\lambda(0) + J_\lambda(z; \sin^2\theta, \cos^2\theta)h_\lambda(0), \tag{5.33}$$

where $J_\lambda(z;a,b) = ae^{i\Delta_1^\lambda z} + be^{i\Delta_2^\lambda z}$ [11; 72], these space variations are to complemented with time variations accordingly (e.g. plane waves).

Consider the situation where gravitational waves only enter the background magnetic field at the $z = 0$, i.e., $h_\lambda(0) = 1$ and $A_\lambda(0) = 0$, then the conversion probability after travelling a distance z inside the background field is

$$P_\lambda(z) = |J_\lambda(z; \sin\theta\cos\theta, -\sin\theta\cos\theta)|^2 \tag{5.34}$$

$$= (\frac{1}{2}\sin 2\theta)^2(e^{i\Delta_1^\lambda z} + e^{i\Delta_2^\lambda z})(e^{-i\Delta_1^\lambda z} - e^{-i\Delta_2^\lambda z}) \tag{5.35}$$

$$= \sin^2 2\theta \sin^2\left(\frac{\Delta_1^\lambda - \Delta_2^\lambda}{2}z\right), \tag{5.36}$$

where the the amplitude of this oscillating probability is directly characterised by the mixing angle θ. If we interpret θ as the mixing angle of neutrinos and Δ's in e.q. 5.34 as neutrino masses, the e.q. 5.34 is of exactly the same structure as in neutrino oscillations for a two-neutrino model, where the matrix S would be interpreted as the neutrino mixing matrix [75].

If the mixing angle is small, i.e. $\Delta_{g\gamma} \ll \Delta_\lambda$ when the graviton-photon coupling is weak, e.q. 5.34 can be approximated as

$$P_\lambda(z) \approx 4\theta^2 \sin^2\left(\frac{m_\lambda}{2}z\right) = 4\theta^2 \sin^2\left(\frac{\pi}{l_{\text{osc}}}z\right), \tag{5.37}$$

where we define the characteristic oscillation length $l_{\text{osc}} = \frac{2\pi}{m_\lambda}$. For $l_{\text{osc}} \gg z$, P can rearranged in a form convenient for estimation.

$$P_\lambda \approx 4\theta^2 \frac{\pi^2}{l_{\text{osc}}^2} z^2 = \Delta_{g\gamma}^2 z^2. \tag{5.38}$$

Although we tend to assume that the background magnetic field is uniform, but in practice, this is only valid up to a scale referred as the coherence/correlation length l_{cor}. For a large propagation distance $z > l_{\text{cor}}$, instead of e.q. 5.38, e.q. 5.37 can be approximated by taking the average of the oscillation factor [73], and hence

$$P_\lambda \approx \frac{\kappa}{4} B_0^2 \left(\frac{l_{\text{osc}}}{l_{\text{cor}}}\right)^2 z^2, \text{ valid if } z > l_{\text{cor}}. \tag{5.39}$$

5.3 Perturbative treatment of inhomogeneities

Results derived in the previous section are in principle only valid for some homogeneous magnetic field (up to some correlation length). But we can introduce small inhomogeneities into the originally homogeneous magnetic field $B_0 =$ constant $\to$ $B(z)$ and perturbatively treat the altered version of e.q. 5.26, where both $\Delta_{g\gamma}$ and Δ_λ become position dependent due to their implicit dependence on $B(z)$.

The arbitrariness in the position dependence of $B(z)$ makes the new differential equations difficult to solve straightforwardly as before. Instead, we rearrange e.q. 5.26 into a form identical to Schrodinger equation

$$i\partial_z\psi_\lambda(z) = (H_{0,\lambda} + H_I)\psi_\lambda(z), \tag{5.40}$$

where the original "Hamiltonian" H_0 and the perturbation "Hamiltonian" H_I are

$$H_{0,\lambda} = -\begin{pmatrix} \Delta_\lambda + \omega & 0 \\ 0 & \omega \end{pmatrix}, \tag{5.41}$$

$$H_I = -\begin{pmatrix} \Delta_{g\gamma} & 0 \\ 0 & \Delta_{g\gamma} \end{pmatrix}. \tag{5.42}$$

This set of "Schrodinger" equations determine the position evolution of $\psi_\lambda(z)$ and can be solved without the perturbation, i.e. when $\Delta_{g\gamma} \to 0 \Rightarrow H_I \to 0$, by the usual quantum mechanics technique [71]

$$\psi_\lambda(z) = U(z)\psi_\lambda(0), \tag{5.43}$$

where the "unitary operator" $U(z)$ is

$$U(z) = e^{-i\int_0^z H_{0,\lambda}(z')dz'}. \tag{5.44}$$

Now treat the perturbation in the "interaction picture"

$$\psi_\lambda^{\text{int}} = U_{0,\lambda}^\dagger \psi_\lambda, \tag{5.45}$$

$$H_{\text{int}}^\lambda = U_{0,\lambda}^\dagger H_I U_{0,\lambda}, \tag{5.46}$$

so that the differential equations can be solved by Dyson's series, with the first order perturbation of the form [71]

$$\psi_\lambda^{\text{1st Pert}}(z) = -i\int_0^z H_{\text{int}}(z')\psi_\lambda(0)dz'. \tag{5.47}$$

Hence, the graviton-photon conversion probability for inhomogeneous magnetic field has the following general form [71; 76]:

$$P_\lambda^{\text{inhom}} = \left|\int_0^z \Delta_{g\gamma} e^{-i\int_0^{dz'}\Delta_\lambda(z'')dz''}dz'\right|. \tag{5.48}$$

5.4 Examples of conversion rates at distinct scales

Primordial gravitational waves and cosmic field

The Fermi observations of blazars, the supermassive black holes with emitted jets pointing at us, suggest a lower bound of the cosmic magnetic field of $B_0 \gtrsim 10^{-16}$G from the obtained gamma-ray spectra [77; 78], whereas the upper bound is placed by the CMB observations with the most optimistic estimation of $B_0 \lesssim 10^{-9}$G by

Planck [79]. Despite being heavily suppressed by the weak magnetic field, the graviton-photon conversion propability P can be compensated by the large scale of the system, which can be taken to be, e.g., the Hubble radius $z \sim 4.48 \times 10^3$Mpc.

In this scenario, the photons resulted from the primordial gravitational waves in the dark ages is of particular interest since in the period where P is least suppressed due to the low plasma density of $n_e \sim 10^{-7}\text{cm}^{-3}$, according to e.q. 5.37, since the free ions are mostly bounded into atoms during the recombination era, and the reionisation process due to formation of primordial stars had not yet begun [64]. Assume that the cosmic magnetic field is homogeneous up to $l_{\text{cor}} \sim 1$Mpc, we obtain from e.q. 5.37 [11; 73]

$$P \approx 5.87 \times 10^{-35} \left(\frac{B_0}{1\text{nG}}\right)^2 \left(\frac{\omega}{100\text{GHz}}\right)^2 \left(\frac{10^{-3}\text{cm}^{-3}}{n_e}\right)^2 \left(\frac{D}{1\text{Mpc}}\right) \left(\frac{10\text{kpc}}{l_{\text{cor}}}\right) \tag{5.49}$$

$$= 2.6 \times 10^{-25} \left(\frac{\omega}{100\text{GHz}}\right)^2, \tag{5.50}$$

which shows that primordial gravitational waves with frequency much higher than 100GHz is required to produce detectable signal, which corresponds to the infrared frequency ($10^{12} - 10^{14}$Hz) and above. However, as mentioned in Section 5.1, 10^{21}Hz is roughly the upper bound above which the photons induced by gravitons can decay into fermion pair, so the idealised detection range for high-frequency gravitational waves from cosmic magnetic field via the inverse Gertsenshtein mechanism is around $10^{12} - 10^{21}$Hz [68].

Galactic clusters

The cosmological magnetohydrodynamic simulations [80] show that the typical strength of the magnetic field in a galaxy cluster is around $B_0 \sim 1\mu$G, much stronger than the cosmological one, and its correlation length heavily depends on how and when the magnetic field is formed, which remains an open question. If we assume that the formation of magnetic field is due to phase transition, then the correlation length can take extreme values as large as $l_{\text{cor}} \sim 400$kpc, but a more realistic value typically adopted is around $l_{\text{cor}} \sim 10$kpc [81; 82].

Despite a stronger magnetic field, the plasma density in a cluster is much higher compared to the large cosmological scale structure which contains a large number of voids, so the electron density inside a cluster can reach as high as $n_e \sim 10^{-1} - 10^{-3}\text{cm}^{-3}$. Repeat the calculations in e.q. 5.49 for a large but common galaxy cluster size of 10Mpc:

$$P \approx 5.8 \times 10^{-28} \left(\frac{\omega}{100\text{GHz}}\right)^2, \tag{5.51}$$

which is weaker than the result in e.q. 5.49 due to the higher plasma density.

Neutron star

Neutron stars are ideal compact objects to study the inverse Gertsenshtein mechanism since they are surrounded by a very strong magnetic field of strength $B_s \sim 10^{10} - 10^{13}$G at their surface. However, unlike in the two former situations, the magnetic field around a neutron star decreases as the distance from its centre increases. So we should use instead the conversion rate for inhomogeneous magnetic field e.q. 5.48. According to the Julien-Goldreich model of neutron star [83], the magnetic field outside a neutron star of radius r_0 takes the form:

$$B(r) = \sqrt{\frac{2}{3}} B_s \left(\frac{r}{r_0}\right)^{-3}, \; r_0 < r < R. \tag{5.52}$$

where the maximal extend of the magnetic field $R \approx \frac{2\pi}{\tau}$ for neutron star spinning period τ. This model also predicts that the electron density around an isolated neutron star is [83]

$$n_e(r) = 7 \times 10^{-2} \left(\frac{1\text{s}}{\tau}\right) \left(\frac{B(r)}{1\text{G}}\right) \text{cm}^{-3}. \tag{5.53}$$

Numerical evaluation of e.q. 5.48 shows that the maximal conversion rate is around $P_\lambda^{\text{inhom}} \approx 2 \times 10^{-14}$ in the infrared frequency range for a neutron star of $B_s = 10^{13}$G, $r_0 = 10$km and $T = 1$s [76].

5.5 The exact solutions for constant magnetic field

Since we are mainly interested in HFGWs, the photon wavelengths are usually very short and hence the WKB approximation is valid. But the exact solutions to the coupled differential equations do exist for homogeneous magnetic field: repeating the computations in Section 4.1, we obtain the modified wave equations (here we temporarily switch our convention to $\eta_{\mu\nu} = \text{diag}(+1, -1, -1, -1)$ to keep align with most previous work in solving exactly these equations, the original convention is assumed for the rest of the paper)

$$(\Box + \omega_{pl}^2) A_1 = h_{\times,z} B_0^{(1)}, \tag{5.54}$$

$$(\Box + \omega_{pl}^2) A_2 = -h_{+,z} B_0^{(1)}, \tag{5.55}$$

where the existence of plasma leads to an effective photon mass and, without of generality, we performed a SO(2) transformation in the xy-plane such that $\boldsymbol{B}_0 = (B_0^1, B_0^2) \to \boldsymbol{B}_0 = (B_0, 0)$ [64].

A mathematical trick is to define differently the label for gravitational polarisations $\lambda \in \{+, \times\}$ for electromagnetic vector potential such that $A_+ = -A^2$ and $A_\times = A^1$ [10]. By doing so a general plane wave can be written as $\psi(t, z) = (A\sqrt{\mu_\lambda}, \frac{1}{\kappa} h_\lambda)^T$ with $\kappa = \sqrt{16\pi G}$, which has conserved norm $|\psi(t, z)|^2$ as can be seen from e.q. 5.56 below [10; 65]. Hence the general solution to the wave equations is

$$\psi(t, z) = e^{-i\omega t} e^{iKz} \psi(0, 0) \tag{5.56}$$

where the hermitian mixing matrix K takes the form [10; 65]

$$K = \begin{pmatrix} \mu\sqrt{\omega^2 + (\frac{\kappa B}{1+\mu})^2} & -i\frac{\sqrt{\mu}\kappa B}{1+\mu} \\ i\frac{\sqrt{\mu}\kappa B}{1+\mu} & \sqrt{\omega^2 + (\frac{\kappa B}{1+\mu})^2} \end{pmatrix} = \begin{pmatrix} \mu\omega_{\text{eff}} & -ig \\ ig & \omega_{\text{eff}} \end{pmatrix}, \tag{5.57}$$

where the off-diagonal terms represent the graviton-photon couplings g and the diagonal terms can be considered as an effective frequency ω_{eff} that characterise the oscillation modes in the box [9; 65].

Consider a constant background magnetic field of length in the a box of length Δl in the z-direction. If the plane wave enters the at $t = z = 0$ is purely gravitational, i.e., $\psi(0,0) = (0, \frac{1}{16\pi G}h_{(0)\lambda})^T$ for some initial metric perturbation $h_{(0)\lambda}$, then

$$\psi(t,z) = \frac{e^{-i\omega t}h_{(0)\lambda}}{\kappa}\begin{pmatrix} (e^{iK\Delta l})_{12} \\ (e^{iK\Delta l})_{22} \end{pmatrix}. \tag{5.58}$$

The exponential of the mixing matrix can be expanded as [65]

$$e^{iK\Delta l} = e^{\frac{i}{2}\text{Tr}(K)\Delta l}\left(\cos\left(\frac{\Delta l}{l_{osc}}\right)\mathbf{1} + il_{osc}\sin\left(\frac{\Delta l}{l_{osc}}\right)\left(K - \frac{1}{2}\text{Tr}(K)\mathbf{1}\right)\right), \tag{5.59}$$

where the oscillation length l_{osc} is, again, defined by the difference between the eigenvalues (which are the wavenumbers of the oscillations modes [65]) Δk of K

$$l_{osc} = \frac{2}{|\Delta k|} = \frac{2}{\sqrt{\omega^2(1-\mu)^2 + \kappa^2 B^2}}. \tag{5.60}$$

Hence the conversion probability of a gravitational wave propagating through the box of size Δl with constant background magnetic field is

$$P = \left(|K_{12}|^2 l_{osc}\sin\left(\frac{\Delta l}{l_{osc}}\right)\right), \tag{5.61}$$

assuming a homogeneous medium [64; 65].

Chapter 6

Distortions of the CMB background due to Gertsenshtein effect

In the first 380000 years after the Big Bang, the universe were mostly filled by hot and dense plasma consisting of free electrons, photon and atomic nuclei. Thus, the photons could frequently interact with the free electrons through Thomson scattering. However, the universe expands and hence the average temperature of the universe drops down below ~ 3000K, which occurs around 380000 years after the Big Bang and leads to the recombination: the nuclei started to capture the free electrons to form neutral atoms. With originally free electrons bounded into atomic systems, the photons started to free stream through the universe and hence were decoupled from the electrons. These photons span a wide range of frequency, and those in the frequency range of $\sim 10^{10} - 10^{12}$Hz form the cosmic microwave background (CMB).

The high temperature environment makes the early universe to remain in thermal equilibrium due intense relativistic interactions. As a consequence, the CMB has also a almost uniform temperature distribution and hence its frequency distribution F_eq of CMB is mathematically described by the blackbody spectrum

$$F_{\text{eq}}(\omega, T) = \frac{1}{e^{\frac{\omega}{T}} - 1}, \tag{6.1}$$

where T is the temperature of CMB which is around $T_0 = 2.725$K$= 56.8$GHz nowadays and ω is here the photon (angular) frequency, which are both time dependent even in equilibrium state due to the expansion of the universe.

6.1 Mathematical framework for CMB distortion

However, the possibility of converting gravitons into photons with the presence of background magnetic field may lead to an observable distortion to the CMB spectrum. Taking this effect into account can not only improve the measurements of the CMB itself, but also indirectly infers the presence of high-frequency gravitational waves (HFGWs) of $10^1 - 10^3$GHz, which are not in the sensitivity frequency range of

current or upcoming detectors. This distortion ΔF_γ can be modelled as

$$\Delta F_\gamma(\omega, T) = F_\gamma(\omega, T) - F_{\text{eq}}(\omega, T), \tag{6.2}$$

where $F_\gamma(\omega_p, T)$ is the total photon spectrum. On the other hand, the distribution of gravitons can be defined as

$$F_g(\omega_p, T) = \frac{\pi^4}{15}\left(\frac{T}{\omega}\right)\left(\frac{\Omega_{gw}}{\Omega_\gamma}\right), \tag{6.3}$$

where $\Omega_\gamma = \frac{\pi^2 T^4}{15\rho_c}$ is the energy density spectrum of photons with the standard quartic dependency on T for radiation, Ω_{gw} is previously defined in e.q. 2.43.

Setting up the Boltzmann equations

Consider a system consisting of n particle species, each associated to a distribution function f_i, $i \in (1, 2, ..., n)$. Then the dynamics of each f_i is determined by Boltzmann's equation which takes the general form:

$$\hat{L} f_i = C[f_j], \tag{6.4}$$

where $\hat{L}$ is the Liouville operator, i.e the total derivative with respect to time, and C is the operator characterising the interactions between different species.

Returning back to our system consisting of two particle species: graviton and photon with frequency dependent distributions. Thus the Liouville operator is

$$\hat{L} = \frac{\partial}{\partial t} + \frac{\partial \omega}{\partial t}\frac{\partial}{\partial \omega}. \tag{6.5}$$

As the universe expands with increasing scale factor $a(t)$, the frequency of the CMB photons is redshifted as $\omega(t) \propto a(t)^{-1}$, hence

$$\hat{L} = \frac{\partial}{\partial t} - H\omega\frac{\partial}{\partial \omega}, \tag{6.6}$$

where $H \equiv \frac{1}{a}\frac{da}{dt}$ is the Hubble parameter. The time coordinate t, defined as the age of the universe, can be expressed as an integral over the expansion factor a

$$t = \int_0^a \frac{da'}{a' H(a')}. \tag{6.7}$$

The average temperature of the universe scales like $T(t) \propto a(t)^{-1}$, hence by a change of variable e.q. 6.7 becomes

$$t = -\int_0^T \frac{dT'}{T' H(T')}, \tag{6.8}$$

which allows us the express the Liouville operator in terms of T and ω [10; 73]

$$\hat{L} = -H\left(T\frac{\partial}{\partial T} + \omega_p\frac{\partial}{\partial \omega}\right). \tag{6.9}$$

If we assume that the frequency is nearly invariant at the time scale of the graviton-photon conversion process, then [73]

$$\hat{L} \approx -HT\frac{\partial}{\partial T}. \tag{6.10}$$

On the other hand, the rate of change of abundance in photon should be proportional to the relative abundance of graviton compared to photon, and vice versa. Therefore, the Boltzmann equations for both F_γ and F_g can be explicitly expressed as

$$-HT\frac{\partial}{\partial T}F_{\gamma,g} = \pm(F_g - F_\gamma)\langle\Gamma_{g\gamma}\rangle, \tag{6.11}$$

where $\langle\Gamma_{g\gamma}\rangle$ is the average graviton-photon conversion rate defined via an integral along the line of sight

$$P = \int_{\text{l.o.s}} \langle\Gamma_{g\gamma}\rangle dt, \tag{6.12}$$

for P defined in e.q. 5.34 [10].

Solving the Boltzmann equations

Define $\tilde{F} \equiv \frac{1}{2}(F_\gamma - F_g)$, then

$$-HT\frac{\partial}{\partial T}\tilde{F} = -2\langle\Gamma_{g\gamma}\rangle\tilde{F}, \tag{6.13}$$

which is a first order differential equation in T that is solvable by

$$\tilde{F}(\omega, T) = \tilde{F}(\omega_i, T_i)e^{-2\int_T^{T_i}\frac{dT'}{T'H(T')}\langle\Gamma_{g\gamma}\rangle}, \tag{6.14}$$

for fixed $\frac{\omega}{T}$ and some initial values ω_i and T_i [65].
It turns out that ω_i is not an independent value, since

$$\hat{L}(F_g + F_\gamma) = 0 \tag{6.15}$$

$$\Rightarrow F_g(\omega, T) + F_\gamma(\omega, T) = F_g(\frac{T_i}{T}\omega, T_i) + F_\gamma(\frac{T_i}{T}\omega, T_i), \tag{6.16}$$

i.e. the frequency is redshifted [65; 73], and hence

$$\tilde{F}(\omega, T) = \tilde{F}(\frac{T_i}{T}\omega, T_i)e^{-2\int_T^{T_i}\frac{dT'}{T'H(T')}\langle\Gamma_{g\gamma}\rangle}. \tag{6.17}$$

By changing the variable in e.q. 6.12 using e.q. 6.8, the integral in the exponential of e.q. 6.18 turns out be the same as e.q. 6.12. Thus, e.q. 6.18 can be reexpressed as

$$\tilde{F}(\omega, T) = \tilde{F}(\frac{T_i}{T}\omega, T_i)e^{-P}(\cosh P - \sinh P), \tag{6.18}$$

from which the complete solutions satisfying e.q. 6.5 can be identified [64; 73]

$$F_\gamma(\omega, T) = e^{-P}\left(\cosh(P)F_\gamma(\frac{T_i}{T}\omega, T_i) + \sinh(P)F_g(\frac{T_i}{T}\omega, T_i)\right), \tag{6.19}$$

$$F_g(\omega, T) = e^{-P}\left(\sinh(P)F_\gamma(\frac{T_i}{T}\omega, T_i) + \cosh(P)F_g(\frac{T_i}{T}\omega, T_i)\right). \tag{6.20}$$

Constraint on Ω_{gw}

Since $P \ll 1$ in general, we can expand the functions of P in e.q. 6.19 to simplify the distribution function of photon at present time $T = T_0$

$$F_\gamma(\omega, T_0) = (1 - P)F_{\text{eq}}(\omega_i, T_i) + PF_g(\omega_i, T_i) + O(P^2), \tag{6.21}$$

so that the distortion to the total CMB distribution is directly determined by the distribution of gravitons [73]

$$\Delta F_\gamma(\omega, T_0) = (F_\gamma(\omega_i, T_i) - F_{\text{eq}}(\omega, T))P \tag{6.22}$$

$$\Rightarrow \frac{\Delta F_\gamma(\omega, T_0)}{F_{eq}} = \left[\frac{\pi^4}{15}\left(\frac{T}{\omega}\right)^4\left(\frac{\Omega_{gw}}{\Omega_\gamma}\right)\left(e^{\frac{\omega}{T_0}} - 1\right) - 1\right]. \tag{6.23}$$

Therefore, by measuring the relative distortion to the CMB $\frac{\Delta F_\gamma(\omega,T_0)}{F_{\text{eq}}}$, the energy density spectrum of gravitational wave can be constrained [73]

$$\Omega_{gw} = \frac{15}{\pi^4}\Omega_\gamma\left(P^{-1}\frac{\Delta F_\gamma(\omega, T_0)}{F_{\text{eq}}} + 1\right)\left(\frac{\omega}{T}\right)^4 F_{\text{eq}}(\omega, T_0), \tag{6.24}$$

which can be equivalently expressed in terms of the characteristic constraint in terms of e.q. 2.58.
It is useful to consider both the high frequency and low frequency limits of e.q. 6.22 by regarding the distorted background as an effective black body:

$$\frac{\Delta F_\gamma}{F_{\text{eq}}}(\omega, T) = \frac{F_{\text{eq}}(\omega, T_\gamma) - F_{\text{eq}}(\omega, T)}{F_{\text{eq}}(\omega, T)}. \tag{6.25}$$

In these two limits, F_{eq} and hence $\frac{\Delta F_\gamma}{F_{\text{eq}}}$ are approximated as

$$F_{\text{eq}}(\omega, T) \approx \begin{cases} \frac{T}{\omega},\ \omega \ll T & \text{(Rayleigh-Jeans limit)} \\ e^{-\frac{\omega}{T_0}},\ \omega \gg T & \text{(high frequency limit)} \end{cases} \tag{6.26}$$

$$\Rightarrow \frac{\Delta F_\gamma}{F_{\text{eq}}}(\omega, T_0) \approx \begin{cases} \frac{T_\gamma - T_0}{\omega},\ \omega \ll T_0 & \text{(Rayleigh-Jeans limit)} \\ e^{-\omega\left(\frac{1}{T_0} - \frac{1}{T_\gamma}\right)},\ \omega \gg T_0 & \text{(high frequency limit)} \end{cases}. \tag{6.27}$$

Bound from effective degree of freedom

Apart from the bound e.q. 6.24 derived from the application the inverse Gertsenshtein mechanism to the distortion of the CMB background, there is also the bound from the effective degree of freedom of gravitational waves. In cosmology, the contribution from relativistic particles, e.g. neutrinos and gravitons, to the total energy density of the universe is accounted by the so-called relativistic degrees of freedom N_{eff} [64; 84]. The contribution to N_{eff} from graviton, N_{gw}, can be separated from the rest of N_{eff} and put another bound on Ω_{gw} [84].

The density of SGWBs $\rho_g(T)$ is constrained by

$$\rho_g(T) \lesssim \frac{7}{8}\left(\frac{4}{11}\right)^{\frac{4}{3}} N_{\text{eff}}\rho_\gamma(T), \tag{6.28}$$

for photon density ρ_γ [84]. From relation e.q. 2.43 and assume that the change in Ω_{gw} is small (so that N_{eff} remains constant), we obtain the following upper bound on the spectrum

$$\Omega_{\text{gw}}(T) \lesssim \frac{7}{8}\left(\frac{4}{11}\right)^{\frac{4}{3}} N_{\text{eff}}\Omega_\gamma(T), \tag{6.29}$$

by differentiating both sides of e.q. 6.28 by $\ln f$ and dividing by ρ_c, the measurements from the Planck satellite in 2020 suggest that $N_{\text{gw}} \gtrsim 0.1$ [85].

6.2 Excess radio background from observational evidence

Due to the propagation time of the light, further we observe, higher the energy density due to the expansion of the universe. Previous observations suggest the following redshift relation for the radio temperature T_R:

$$T_R = (1+z)T_0. \tag{6.30}$$

However, the observations from ARCADE2 [86] and EDGES [87] collaborations suggest that there is an excess contribution ΔT to T_R that is empirically modelled as a power law

$$\frac{\Delta T}{T_0} = A_R\left(\frac{\nu_{obs}}{78\text{MHz}}\right) \tag{6.31}$$

where the exponent $\beta \approx -2.6$ is called the spectral index, A_R is a frequency-dependent amplitude, ν is the observed frequency of the radio background, and $78\text{MHz} \ll T_0$ is chosen to be the centre of the flattened absorption frequency profile from EDGES, the first sky-averaged 21 cm absorption observation [64; 73; 87].
With this particular excess background ΔT, e.q. 6.30 becomes

$$T_R = (1+z)T_0\left(1 + A_R\left(\frac{\nu_{obs}}{78\text{MHz}}\right)\right). \tag{6.32}$$

Now take the Rayleigh-Jeans limits which are suitable to describe radio background in e.q. 6.26 and e.q. 6.27 and substitute e.q. 6.31 into the constraint e.q. 6.24, we obtain

$$\Omega_{gw} \approx \frac{15}{\pi^4}\Omega_\gamma\left(P^{-1}A_r\left(\frac{\nu}{78\text{MHz}}\right) + 1\right)\left(\frac{\omega}{T}\right)^3. \tag{6.33}$$

6.3 CMB distortion due to kinematic Sunyaev-Zel'dovich effect

The kinematic Sunyaev-Zel'dovich (kSZ) effect describes the scattering of low energy CMB photons with free electrons, the energy transfers of which cause a shift in

the temperature ΔT_{kSZ} of scattered CMB photons [88]. For a galaxy with electron density n_e moving at peculiar velocity v_p relative to the observer, the observed kSZ temperature shift is computed via a line-of-sight integral over line element dl

$$\frac{T_{\text{kSZ}}}{T_0} = \sigma_T \int_{\text{l.o.s}} e^{-\tau} n_e v_p dl, \tag{6.34}$$

where σ_T is the Thompson scattering and τ is the optical depth along the line-of-sight.

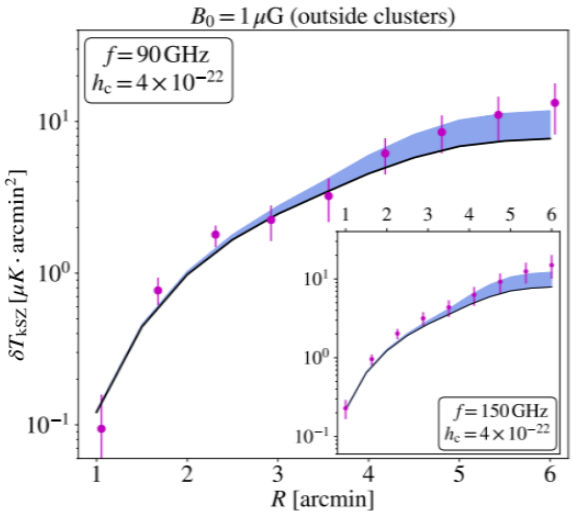

Figure 6.1: A plot illustrating the evolution of the excess temperature as a function of the observation angle for both radio signal frequency of $f = 90$GHz and $f = 150$GHz (at bottom right corner) in an ICM magnetic field of $B_0 = 1\mu$G. The black solid curve indicates the expected CMB distortion δT_{kSZ} due to the kSZ effect modelled by the baryonic content of the galactic cluster, whereas the blue shaded zone indicates the additional excess temperature due the inverse Gertsenshtein mechanism. The purple dots represent the measured data from the ACT radiotelescope. Diagram taken from [73].

The ACT mission observes in near space within a redshift range of $0.4 - 0.7$, hence the optical depth is very short so $e^{-\tau} \sim 1$ [88], and the galaxies observed by ACT has a root-mean-square peculiar velocity of $v_p \approx 1.06 \times 10^{-3}$, hence [73]

$$\frac{T_{\text{kSZ}}}{T_0} \approx 1.06 \times 10^{-3} \sigma_T \int_{\text{l.o.s}} n_e dl. \tag{6.35}$$

The ACT observations show that the kSZ effect dominates the excess in the CMB background at frequency scales 10^{11}GHz, but the inclusion of photons produced by gravitons in ICM magnetic field improves the consistency between the observed data and the theoretical prediction from the baryon physics modelling, as shown in Figure 6.1 [73].

Chapter 7

Direct detection of high-frequency gravitational waves using Gertsenshtein effect

7.1 Axion detectors

After the discovery of the strong interaction, the theorists soon realised that the QCD vacuum needs to process a complicated structure to explain the missing of the $U(1)_{\mathrm{A}}$ axial symmetry, which itself cannot explain why the Charge-Parity (CP) symmetry is not badly broken in this new QCD vacuum and it is known as the strong CP problem [89]. To solve this problem, Peccei and Quinn proposed in 1977 to introduce a chiral $U(1)_{\mathrm{C}}$ symmetry to the Standard Model, the spontaneous breaking of which results in a Goldstone boson named axions which carry an effective potential with vanishing CP symmetry breaking at the minimum and hence solve the strong CP problem [90].

Apart from solving the strong CP problem, axions are also considered as one of the major candidates of dark matter [46]. The detection of axions and other axion-like particles (ALPs) relies on one of the defining properties of axions: axions and photons can convert into each other in the presence of an external magnetic field, which is a mathematically equivalent process to the Gertsenshtein effect (but Gersenshtein effect does not involve any beyond Standard Model physics).

The currently existing axion detectors, such as the CAST & OSQAR experiments at CERN and the ALPS experiment at DESY, all share a similar design. The main structure of these detectors consists of a cavity sandwiched between strong magnets that produce a strong magnetic field orthogonal to the latters of strength $\sim 1 - 10$T. The incoming axions are converted into photons which are then captured by the detector behind the cavity and converted into light signals. Among the three detectors mentions, CAST is a helioscope that attempts to capture axions emitted by the Sun, whereas the other two produce axions in another cavity with identically strong magnetic field by sending in strong photon beams. [91].

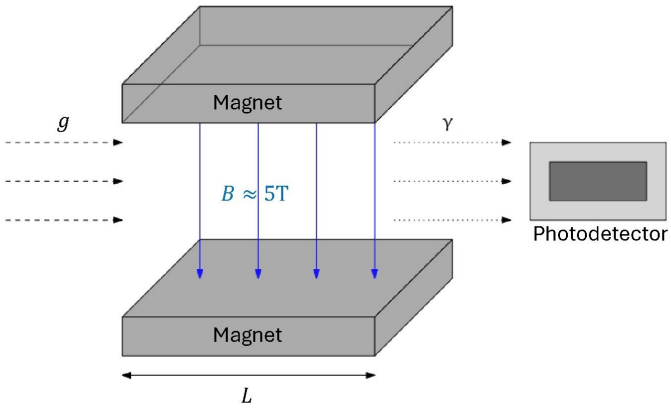

Figure 7.1: A diagrammatic illustration of how a cavity of an axion detector could be used for direct gravitational wave detection by the Gertsenshtein effect. The incoming gravitational waves are converted to photons after passing through this cavity which has inside a magnetic field of $B_0 \approx 5\mathrm{T}$ and is originally designed to convert axions into photons. A charge couple device photodetector located behind the cavity is used to capture the induced photons.

In principle, these axion detectors could also be used for gravitational wave detection by using their strong magnetic fields [92]. Although there is currently no results for constraining gravitational waves based the data collected by these detectors, we can estimate the potential constraint on the gravitational strain by considering the graviton-induced energy flux of photons hitting the detector. The photon flux $\Phi(t,z)$ at a point z (along the direction orthogonal to the magnetic fields) is determined by the local electric field of generated photons [91]:

$$\Phi(t,z) \equiv \sum_{\lambda} \langle |E_\lambda(t,z)|^2 \rangle. \tag{7.1}$$

Electric field components $E_\lambda(t,z)$ on the right-hand-side can be converted into vector potential $A_\lambda(t,z)$, and by assuming that the time evolution of $A_\lambda(t,z)$ (complementary to e.q. 5.32) is plane-wave like, we have in Fourier space [91]

$$E_\lambda(t,z) = -\partial_t A_\lambda(t,z) = i\omega \int_{-\infty}^{\infty} \frac{d\omega}{2\pi} \int d^2\hat{\Omega} A_\lambda(\omega,\hat{\Omega}) e^{-i\omega t}. \tag{7.2}$$

On the other hand, by substituting the results in e.q. 2.55 & e.q. 2.58 in e.q. 2.53, we have

$$\langle h_{ij}(t,0) h_{ij}(t,0) \rangle = 4 \int_0^{\infty} \frac{d\ln\omega}{2\pi} \omega S_{\mathrm{gw}}(\omega) = 4 \int_0^{\infty} \frac{d\ln\omega}{2\pi} (h_c(\omega))^2. \tag{7.3}$$

Hence by converting A_λ in h_λ using e.q. 5.32 and substituting e.q. 7.2 into e.q. 7.1, we can express the photon flux in terms of the characteristic strain h_c

$$\Phi(t,z) = \frac{1}{4\kappa^2}\int_0^\infty (h_c(\omega))^2 \sum_\lambda |J_\lambda(z; \sin\theta\cos\theta, -\sin\theta\cos\theta)|^2 \omega d\omega \tag{7.4}$$

$$= \frac{1}{4\kappa^2}\int_0^\infty h_c^2 \sum_\lambda P_\lambda(z)\omega d\omega, \tag{7.5}$$

where for the very small distance z inside the detector such that $l_{\text{osc}} \gg z$, we approximately have using e.q. 5.37

$$\Phi(t,z) = \int_0^\infty \frac{B_0^2 z^2}{4} h_c^2 \omega d\omega. \tag{7.6}$$

To obtain the constraint on h_c, we need to compare e.q. 7.1 to the minimum photon flux required for Charge Couple Device (CCD) photodetector which sensitive in some energy bandwidth $\omega_l < \omega < \omega_h$ with an efficiency η_γ and a cross section A [91]

$$\Phi(t,z)^{\text{CCD}} = \int_{\omega_l}^{\omega_h} \frac{1}{A}\frac{N(t,\omega)}{\eta_\gamma(\omega)}\omega d\omega. \tag{7.7}$$

Hence by detecting any meaningful gravitational wave signals, i.e. for $\Phi(t,z) \geq \Phi(t,z)^{\text{CCD}}$ in the same energy bandwidth, we have the following constraint on h_c

$$h_c^2(\omega) \geq \frac{4N(t,\omega)}{B_0^2 L^2 A \eta_\gamma(\omega)}. \tag{7.8}$$

The Peccei-Quinn theory also predicts that an axion can decay into a pair of gravitons and hence should contribute directly to the gravitational background of the universe, hence gravitational waves from, e.g. axion cloud around compact astrophysical objects, are suggested as a probe of axions [93]. However, inside a detector, such axion-induced graviton should not have any significant contribution since axion-to-graviton and Gertsenshtein effect are both suppressed processes.

7.2 Superconducting radio-frequency cavity: MAGO

MAGO is an experiment currently under construction based on the interaction between electromagnetic (inverse Gertsenshtein effect) and mechanical (strain) resonances aiming to detect high-frequency [95; 96] gravitational. The typical detection range of the MAGO detector is around 10kHz to 1GHz with a characteristic strain of $h \sim 10^{-18} - 10^{-22}$, which is right above the detection range of current ground-based detectors [95]. The cavity consists of two sueprconducting nearly spherical subcavities connected by a central tuning cell, such two coupled-sphere design makes the detector having two electromagnetic eigenmodes corresponding to two resonant frequencies ω_0 and ω_1 at which the cavities store electromagnetic energy, with the frequency gap $\Delta\omega = \omega_1 - \omega_0$ that can be tuned by adjusting the connecting cell [95].

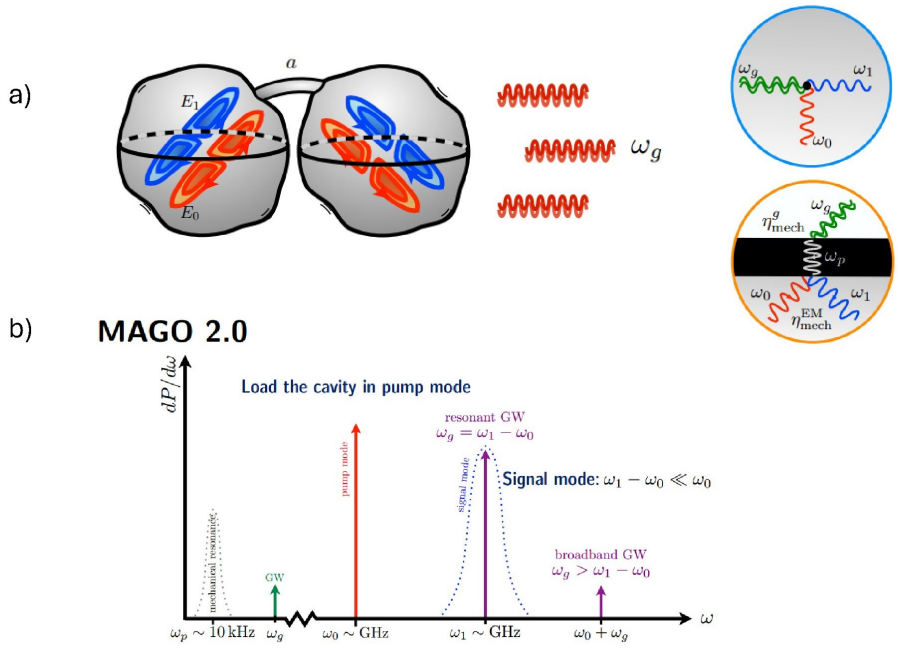

Figure 7.2: The top diagram a) illustrates the design of the MAGO detector, where the orange curves represent the pump mode and the blue ones represent the signal mode, which are both resonant modes of the electromagnetic waves inside the cavities and can be tuned by adjusting the length a of the cell connecting the two cavities. The two onsets respectively show the direct coupling (top right, in blue circle) and the indirect coupling (top left, in orange circle) between the incoming gravitational waves of frequency ω_g and the electromagnetic resonant modes of the cavities. The bottom plot b) shows the various frequency modes of the electromagnetic (red and purple)/gravitational (green)/mechanical waves (black) and their corresponding differential powers $\frac{dP}{d\omega}$ with respect to the frequency ω. Diagram and plot taken from the workshop presentation [94].

Initially, the cavity stored electromagnetic energy at the lower frequency mode ω_0, referred as the pump mode, by connecting to an external radio oscillator. When gravitational wave signal of frequency $\omega_g \sim \Delta\omega$ enters the cavity, ideally by the inverse Gertsenshtein effect, the graviton-induced photons excite the pump mode to the higher signal mode, which is referred as the direct coupling of gravitational and electromagnetic waves [96]. Hence detecting this shift to the signal mode implies the detection of the gravitational waves.

However, another indirect coupling is expected in practice: the gravitational wave causes the mechanical vibration of the cavity shape at frequency ω_p which can be tuned by the shape of the cavity, and this mechanical vibration in turns causes the excitation of both the pump and the signal modes [96]. The mixing of direct and indirect coupling significantly enhances the sensitivity of the cavity to detect high frequency gravitational waves. To properly study the deformation of the cavity and

interaction of gravitational and mechanical couplings due to the presence of gravitational waves, one needs to first properly understand and apply the cavity perturbation theory, which is beyond the scope of this dissertation, interested reader is referred to [96] for mathematical details.

Just as how the axion detectors can be used for gravitational wave detection, MAGO can also be used for axion detection as well [95]. All these suggest that the future high-frequency gravitational wave detectors and axion detectors should be designed to be multi-purposed, which can bring together efforts from different communities for interdisciplinary research.

7.3 Other experiments for high-frequency gravitational wave detection

Other then the two categories of detectors for high-frequency gravitational wave detection based on the inverse Gertsenshtein mechanism mentioned above, there are some other concepts and designs for high-frequency gravitational detection. We briefly introduce a couple of representative ones in this section.

Levitated sensor detectors

The current ground based interferometric detectors (LVK) have very limited sensitivity on the detection of high-frequency gravitational waves due to the photon shot noise that rises with frequency. Thus, it is still possible to detect high-frequency gravitational waves using detector with similar structure to LVK but with a different way of measuring the impact of spacetime perturbation.

Instead of considering the change in the length of Fabry-Perot arms, an alternative approach is to consider a similar inteferometer with a small dielectric sensor between the mirrors of an arm. Each arm has a laser travelling along the former and hence produces a standing wave that traps this dielectric sensor located at an antinode [97]. When a gravitational wave travel through the interferometer, the trapped sensor is subject to a force that can resonantly excited by matching the strain to the natural frequency ω_0 of the system. This natural frequency is determined by the optical potential U of the laser and hence can be flexibly adjusted by changing the laser intensity:

$$\omega_0^2 = \frac{1}{M}\frac{d^2U}{dz^2}(z_s), \tag{7.9}$$

for a dielectric sensor of mass M and position z_s along the arm (set to be z-axis) [98].

The sensitivity of this new detector is mainly affected by the thermal noise, such as the recoil of the sensor due to presence of photons, and hence the main challenge is to keep the thermal noise low while increaseing the sensitivity of the, i.e. lower the minimum detectable h_c which is inversely proportional to M (roughly for

vacuum) [97; 98]. Therefore, it is important to appropriately choose the geometry of the sensor, current suggestions include a stack of thin-layered dielectric discs [98] and silicon nitride (SiN) membrane [99], these configurations usually lead to a sensitivity range $\gtrsim 10$kHz and up to ~ 100MHz.

Bulk Acoustic Wave devices

The detection methods discussed above are mainly based on optical devices with electromagnetic modes to be excited by gravitational waves, but there are also plans to detect gravitational waves by exciting acoustic modes, such as MAGE (Australian [100]) and BAUSCIA (Italian [101]) experiments. The main idea is to employ a bulk acoustic wave (BAW) device made of piezoelectric materials which generate acoustic waves (phonons) when experiencing change in the electric field. This BAW device is connected in a DC circuit and hence the strain caused by the gravitational waves would make the BAW device to emit acoutic waves, which are then amplified by superconducting quantum interference devices (SQUIDs) [100]. The BAW device also has a natural resonance frequency that can be adjusted to match that of the gravitational waves. Compared to the optical resonator such as the levitated sensor detectors, this kind of acoustic resonator has a higher sensitivity range that can reach GeV scales because of its high mechanical quality factors [100].

Chapter 8

Summary & Outlook

In this dissertation, we had a qualitative discussion on the various sources of HFGWs, which shows that HFGWs are closely related to primordial black holes, the evolution of the early universe and beyond Standard Model high-energy physics. A particular emphasis is given to the potential detectability and the expected frequency range of each of these sources. These connections between HFGWs and different vital aspects of the modern fundamental physics justify the importance of detecting the formers that are beyond the reach of current detectors and hence make the Gertsenshtein mechanism, a frequency-independent process directly derived from general relativity, of particular interests for designing future HFGW detection experiments.

The Gertsenshtein effect (graviton to photon) and its inverse process (photon to graviton) are respectively derived from the Einstein equations and the Maxwell equation in curved spacetime, where the components of metric perturbation and electromagnetic vector potential are mutually coupled in these differential equations. However, despite being ignored in most literature, the rigorous treatment of electric and magnetic fields in curved spacetime requires the extra contributions from the metric, which, nonetheless, does not affect the final differential equations for homogeneous magnetic field that we assume in most scenarios. Nonetheless, the treatment of inhomogeneous magnetic field in the Gertsenshtein mechanism is still possible by perturbatively treating the differential equations obtained in the homogeneous case, which are to be solved by noticing the similarity between the differential equation and the Schrodinger equation.

In actual astrophysical/cosmological scenarios, the space is filled by plasma which induces the birefringe effects to propagating electromagnetic waves due to the presence of a background magnetic field pointing in some particular direction. To describe the Gertsenshtein mechanism in a such setting, an effective theory based on the self-interaction of photons was built to take into account QED effects (namely the self-interaction of photons) as well as the change in refractive index due to plasma and birefringes. The resulting equations of motions are usually solved in the framework of the WKB approximation by assuming short photon wavelength relative to correlation length of the magnetic field, although the exact solution that is mathematically lengthy to obtained does exist for homogeneous magnetic fields. By solving

how different components of the metric perturbation and electromagnetic vector potential evolve, we showed via a series of concrete examples that the photon-graviton conversion is usually a very suppressed process due to either the insufficient magnetic field strength or the limitation of the spatial scales.

Because of the presence of the cosmological magnetic fields, the Gertsenshtein effect is expected to contribute the excess of the CMB background, despite having a relatively weaker contribution relative to the kSZ effect. However, if confirming the CMB distortions due to the Gertsenshtein effect, the spectral shape and the energy density of SGWBs can be constrainted to a even higher precision, and the properties of HFGWs along with their sources can be indirectly inferred from the observations of the existing radiotelescopes.

Most importantly, the Gertsenshtein mechanism enables new opportunities for the direct detection of HFGWs, which can be achieved by using current axion detectors since the mutual conversion of axions and photons in background magnetic field is an equivalent process to the Gertsenshtein mechanism. This equivalency suggests that the future detectors of HFGWs or axions should be designed to be multi-purposed in the stage of instrumentation, which naturally bridges the search for HFGWs and high-energy physics beyond the Standard Model of particle physics. Meanwhile, new detectors based on the Gertsenshtein mechanism are also in the conception or construction stage, such as MAGO which amplifies the signals of HFGWs by the the resonance of the graviton-induced electromagnetic waves and the mechanical vibration of the cavities, other detectors based on similar resonances could also be conceptualised. Alongside with other proposed detectors aiming for HFGWs and other next-generation detectors looking for signals in lower frequency ranges, we are stepping into an exciting era of exploring various aspects of fundamental physics that interweave with each other via the detection of gravitational wave signals in frequency ranges unreachable previously.

Bibliography

[1] Abbott BP, Abbott R, Abbott TD, Abernathy MR, Acernese F, Ackley K, et al. Observation of Gravitational Waves from a Binary Black Hole Merger. Phys Rev Lett. 2016 Feb;116:061102. Available from: https://link.aps.org/doi/10.1103/PhysRevLett.116.061102. doi:10.1103/PhysRevLett.116.061102.

[2] Aggarwal N, Aguiar OD, Bauswein A, Cella G, Clesse S, Cruise AM, et al. Challenges and opportunities of gravitational-wave searches at MHz to GHz frequencies. Living Reviews in Relativity. 2021 Dec;24(1). Available from: http://dx.doi.org/10.1007/s41114-021-00032-5. doi:10.1007/s41114-021-00032-5.

[3] Domcke V. Electromagnetic high-frequency gravitational wave detection; 2023.

[4] Domcke V, Kopp J. Electromagnetic (high-frequency) gravitational wave detectors: Interferometers revisited; 2024.

[5] Gertsenshtein ME. Wave resonance of light and gravitational waves. Zh Eksp Theor Fiz. 1962;14:84-5. Available from: http://jetp.ras.ru/cgi-bin/dn/e_014_01_0084.pdf.

[6] Lupanov GA. A capacitor in the field of a gravitational wave. Zh Eksp Theor Fiz. 1967;25:76. Available from: http://jetp.ras.ru/cgi-bin/dn/e_025_01_0076.pdf.

[7] Boccaletti D, De Sabbata V, Fortini P, GVALI C. Conversion of photons into gravitons and vice versa in a static electromagnetic field. Nuovo Cimento B (1965-1970). 1970;70:129-46. doi:https://doi.org/10.1007/BF02710177.

[8] Zel'dovich YB. Electromagnetic and gravitational waves in a stationary magnetic field. Journal of Experimental and Theoretical Physics. 1973;65:1311-5. Available from: http://www.jetp.ac.ru/cgi-bin/e/index/150/6?a=list.

[9] Liu T, Ren J, Zhang C. Limits on High-Frequency Gravitational Waves in Planetary Magnetospheres. Physical Review Letters. 2024 Mar;132(13). Available from: http://dx.doi.org/10.1103/PhysRevLett.132.131402. doi:10.1103/physrevlett.132.131402.

[10] Domcke V, Garcia-Cely C. Potential of Radio Telescopes as High-Frequency Gravitational Wave Detectors. Physical Review Letters. 2021 Jan;126(2). Available from: http://dx.doi.org/10.1103/PhysRevLett.126.021104. doi:10.1103/physrevlett.126.021104.

[11] Dolgov AD, Ejlli D. Conversion of relic gravitational waves into photons in cosmological magnetic fields. Journal of Cosmology and Astroparticle Physics. 2012 Dec;2012(12):003–003. Available from: http://dx.doi.org/10.1088/1475-7516/2012/12/003. doi:10.1088/1475-7516/2012/12/003.

[12] Gauntlett J. General Relativity [Lecture]. London,UK: Imperial College London; 2023.

[13] Hartle JB. In: An Introduction to Einstein's General Relativity. Addison Wesley; 2003. .

[14] Dirkes A. Gravitational waves — A review on the theoretical foundations of gravitational radiation. International Journal of Modern Physics A. 2018 May;33(14n15):1830013. Available from: http://dx.doi.org/10.1142/S0217751X18300132. doi:10.1142/s0217751x18300132.

[15] Riles K. Gravitational waves: Sources, detectors and searches. Progress in Particle and Nuclear Physics. 2013 Jan;68:1–54. Available from: http://dx.doi.org/10.1016/j.ppnp.2012.08.001. doi:10.1016/j.ppnp.2012.08.001.

[16] Poisson E. Gravitational waves from inspiraling compact binaries: The quadrupole-moment term. Physical Review D. 1998 Apr;57(8):5287–5290. Available from: http://dx.doi.org/10.1103/PhysRevD.57.5287. doi:10.1103/physrevd.57.5287.

[17] Blanchet L. Gravitational Radiation from Post-Newtonian Sources and Inspiralling Compact Binaries. Living Reviews in Relativity. 2014 Feb;17(1). Available from: http://dx.doi.org/10.12942/lrr-2014-2. doi:10.12942/lrr-2014-2.

[18] Saulson PR. In: The Search for Gravitational Waves. World Scientific Publishing Co Pte Ltd; 2017. p. 1-8. Available from: https://worldscientific.com/doi/abs/10.1142/9789813146198_0001. doi:10.1142/9789813146198_0001.

[19] Hulse RA, Taylor JH. Discovery of a pulsar in a binary system. Astrophys J Lett. 1975;195:L51-3. doi:10.1086/181708.

[20] Damour T. 1974: the discovery of the first binary pulsar. Classical and Quantum Gravity. 2015 Jun;32(12):124009. Available from: http://dx.doi.org/10.1088/0264-9381/32/12/124009. doi:10.1088/0264-9381/32/12/124009.

[21] Taylor JH, Fowler LA, McCulloch PM. Measurements of general relativistic effects in the binary pulsar PSR1913 + 16. Nature. 1979 Feb;277(5696):437-40. Available from: https://doi.org/10.1038/277437a0. doi:10.1038/277437a0.

[22] Damour T, Taylor JH. On the Orbital Period Change of the Binary Pulsar PSR 1913+16. . 1991 Jan;366:501. doi:10.1086/169585.

[23] Auclair P, et al. Cosmology with the Laser Interferometer Space Antenna. Living Rev Rel. 2023;26(1):5. doi:10.1007/s41114-023-00045-2.

[24] Allen B, Romano JD. Detecting a stochastic background of gravitational radiation: Signal processing strategies and sensitivities. Phys Rev D. 1999 Mar;59:102001. Available from: https://link.aps.org/doi/10.1103/PhysRevD.59.102001. doi:10.1103/PhysRevD.59.102001.

[25] Contaldi C. Stochastic gravitational wave backgrounds [Lecture]. Valencia, Spain: University of Valencia; 2023.

[26] Abbott BP, Abbott R, Adhikari R, Ajith P, Allen B, Allen G, et al. LIGO: the Laser Interferometer Gravitational-Wave Observatory. Reports on Progress in Physics. 2009 Jun;72(7):076901. Available from: http://dx.doi.org/10.1088/0034-4885/72/7/076901. doi:10.1088/0034-4885/72/7/076901.

[27] Acernese F, Agathos M, Agatsuma K, Aisa D, Allemandou N, Allocca A, et al. Advanced Virgo: a second-generation interferometric gravitational wave detector. Classical and Quantum Gravity. 2014 Dec;32(2):024001. Available from: http://dx.doi.org/10.1088/0264-9381/32/2/024001. doi:10.1088/0264-9381/32/2/024001.

[28] Akutsu T, Ando M, Arai K, Arai Y, Araki S, Araya A, et al. KAGRA: 2.5 generation interferometric gravitational wave detector. Nature Astronomy. 2019 Jan;3(1):35–40. Available from: http://dx.doi.org/10.1038/s41550-018-0658-y. doi:10.1038/s41550-018-0658-y.

[29] Punturo M, Abernathy M, Acernese F, Allen B, Andersson N, Arun K, et al. The Einstein Telescope: a third-generation gravitational wave observatory. Classical and Quantum Gravity. 2010 sep;27(19):194002. Available from: https://dx.doi.org/10.1088/0264-9381/27/19/194002. doi:10.1088/0264-9381/27/19/194002.

[30] Reitze D, Adhikari RX, Ballmer S, Barish B, Barsotti L, Billingsley G, et al.. Cosmic Explorer: The U.S. Contribution to Gravitational-Wave Astronomy beyond LIGO; 2019. Available from: https://arxiv.org/abs/1907.04833.

[31] Amaro-Seoane P, Audley H, Babak S, Baker J, Barausse E, Bender P, et al.. Laser Interferometer Space Antenna; 2017. Available from: https://arxiv.org/abs/1702.00786.

[32] Luo Z, Wang Y, Wu Y, Hu W, Jin G. The Taiji program: A concise overview. Progress of Theoretical and Experimental Physics. 2020 07;2021(5):05A108. Available from: https://doi.org/10.1093/ptep/ptaa083. doi:10.1093/ptep/ptaa083.

[33] Luo J, Chen LS, Duan HZ, Gong YG, Hu S, Ji J, et al. TianQin: a space-borne gravitational wave detector. Classical and Quantum Gravity. 2016 Jan;33(3):035010. Available from: http://dx.doi.org/10.1088/0264-9381/33/3/035010. doi:10.1088/0264-9381/33/3/035010.

[34] Amaro-Seoane P, Audley H, Babak S, Baker J, Barausse E, Bender P, et al.. Laser Interferometer Space Antenna; 2017. Available from: https://arxiv.org/abs/1702.00786.

[35] Mentasti G, Contaldi CR, Peloso M. Probing the galactic and extragalactic gravitational wave backgrounds with space-based interferometers. JCAP. 2024;06:055. doi:10.1088/1475-7516/2024/06/055.

[36] Antoniadis J, Babak S, Bak Nielsen AS, Bassa CG, Berthereau A, Bonetti M, et al. The second data release from the European Pulsar Timing Array: I. The dataset and timing analysis. Astronomy amp; Astrophysics. 2023 Oct;678:A48. Available from: http://dx.doi.org/10.1051/0004-6361/202346841. doi:10.1051/0004-6361/202346841.

[37] Agazie G, Anumarlapudi A, Archibald AM, Arzoumanian Z, Baker PT, Bécsy B, et al. The NANOGrav 15 yr Data Set: Evidence for a Gravitational-wave Background. The Astrophysical Journal Letters. 2023 Jun;951(1):L8. Available from: http://dx.doi.org/10.3847/2041-8213/acdac6. doi:10.3847/2041-8213/acdac6.

[38] Reardon DJ, Shannon RM, Cameron AD, Goncharov B, Hobbs GB, Middleton H, et al. The Parkes pulsar timing array second data release: timing analysis. Monthly Notices of the Royal Astronomical Society. 2021 Aug;507(2):2137–2153. Available from: http://dx.doi.org/10.1093/mnras/stab1990. doi:10.1093/mnras/stab1990.

[39] Maiorano M, De Paolis F, Nucita A. Principles of Gravitational-Wave Detection with Pulsar Timing Arrays. Symmetry. 2021 Dec;13(12):2418. Available from: http://dx.doi.org/10.3390/sym13122418. doi:10.3390/sym13122418.

[40] Aggarwal N, Aguiar OD, Bauswein A, Cella G, Clesse S, Cruise AM, et al. Challenges and opportunities of gravitational-wave searches at MHz to GHz frequencies. Living Reviews in Relativity. 2021 Dec;24(1). Available from: http://dx.doi.org/10.1007/s41114-021-00032-5. doi:10.1007/s41114-021-00032-5.

[41] Nakamura T, Sasaki M, Tanaka T, Thorne KS. Gravitational Waves from Coalescing Black Hole MACHO Binaries. The Astrophysical Journal. 1997

Oct;487(2):L139–L142. Available from: http://dx.doi.org/10.1086/310886. doi:10.1086/310886.

[42] Cheek A, Heurtier L, Perez-Gonzalez YF, Turner J. Evaporation of primordial black holes in the early Universe: Mass and spin distributions. Physical Review D. 2023 Jul;108(1). Available from: http://dx.doi.org/10.1103/PhysRevD.108.015005. doi:10.1103/physrevd.108.015005.

[43] Dong R, Kinney WH, Stojkovic D. Gravitational wave production by Hawking radiation from rotating primordial black holes. Journal of Cosmology and Astroparticle Physics. 2016 Oct;2016(10):034–034. Available from: http://dx.doi.org/10.1088/1475-7516/2016/10/034. doi:10.1088/1475-7516/2016/10/034.

[44] Brito R, Cardoso V, Pani P. Superradiance: New Frontiers in Black Hole Physics. Springer International Publishing; 2020. Available from: http://dx.doi.org/10.1007/978-3-030-46622-0. doi:10.1007/978-3-030-46622-0.

[45] Arvanitaki A, Dubovsky S. Exploring the string axiverse with precision black hole physics. Physical Review D. 2011 Feb;83(4). Available from: http://dx.doi.org/10.1103/PhysRevD.83.044026. doi:10.1103/physrevd.83.044026.

[46] Chadha-Day F, Ellis J, Marsh DJE. Axion Dark Matter: What is it and Why Now?; 2022. Available from: https://arxiv.org/abs/2105.01406.

[47] Maria Chiara G, Nicola B, Michele L, Sabino M. Gravitational waves from inflation. La Rivista del Nuovo Cimento. 2016 Aug;39(9):399–495. Available from: https://doi.org/10.1393/ncr/i2016-10127-1. doi:10.1393/ncr/i2016-10127-1.

[48] Bartolo N, Caprini C, Domcke V, Figueroa DG, Garcia-Bellido J, Guzzetti MC, et al. Science with the space-based interferometer LISA. IV: probing inflation with gravitational waves. Journal of Cosmology and Astroparticle Physics. 2016 Dec;2016(12):026–026. Available from: http://dx.doi.org/10.1088/1475-7516/2016/12/026. doi:10.1088/1475-7516/2016/12/026.

[49] Allahverdi R, Brandenberger R, Cyr-Racine FY, Mazumdar A. Reheating in Inflationary Cosmology: Theory and Applications. Annual Review of Nuclear and Particle Science. 2010 Nov;60(1):27–51. Available from: http://dx.doi.org/10.1146/annurev.nucl.012809.104511. doi:10.1146/annurev.nucl.012809.104511.

[50] Brandenberger R, Delgado PCM, Ganz A, Lin C. Graviton to photon conversion via parametric resonance. Physics of the Dark Universe. 2023 May;40:101202. Available from: http://dx.doi.org/10.1016/j.dark.2023.101202. doi:10.1016/j.dark.2023.101202.

[51] Dufaux JF, Bergman A, Felder G, Kofman L, Uzan JP. Theory and numerics of gravitational waves from preheating after inflation. Physical Review D.

2007 Dec;76(12). Available from: http://dx.doi.org/10.1103/PhysRevD.76.123517. doi:10.1103/physrevd.76.123517.

[52] Mazumdar A, White G. Review of cosmic phase transitions: their significance and experimental signatures. Reports on Progress in Physics. 2019 Jun;82(7):076901. Available from: http://dx.doi.org/10.1088/1361-6633/ab1f55. doi:10.1088/1361-6633/ab1f55.

[53] Athron P, Balázs C, Fowlie A, Morris L, Wu L. Cosmological phase transitions: From perturbative particle physics to gravitational waves. Progress in Particle and Nuclear Physics. 2024 Feb;135:104094. Available from: http://dx.doi.org/10.1016/j.ppnp.2023.104094. doi:10.1016/j.ppnp.2023.104094.

[54] Caprini C, Hindmarsh M, Huber S, Konstandin T, Kozaczuk J, Nardini G, et al. Science with the space-based interferometer eLISA. II: gravitational waves from cosmological phase transitions. Journal of Cosmology and Astroparticle Physics. 2016 Apr;2016(04):001–001. Available from: http://dx.doi.org/10.1088/1475-7516/2016/04/001. doi:10.1088/1475-7516/2016/04/001.

[55] Dunsky DI, Ghoshal A, Murayama H, Sakakihara Y, White G. GUTs, hybrid topological defects, and gravitational waves. Phys Rev D. 2022;106(7):075030. doi:10.1103/PhysRevD.106.075030.

[56] Blanco-Pillado JJ, Cui Y, Kuroyanagi S, Lewicki M, Nardini G, Pieroni M, et al.. Gravitational waves from cosmic strings in LISA: reconstruction pipeline and physics interpretation; 2024. Available from: https://arxiv.org/abs/2405.03740.

[57] Øyvind Christiansen, Adamek J, Hassani F, Mota DF. Gravitational waves from dark domain walls; 2024. Available from: https://arxiv.org/abs/2401.02409.

[58] Frolov A, Kofman L. Gravitational Waves from Braneworld Inflation; 2002. Available from: https://arxiv.org/abs/hep-th/0209133.

[59] Palessandro A, Rothman T. A simple derivation of the Gertsenshtein effect. Physics of the Dark Universe. 2023 May;40:101187. Available from: http://dx.doi.org/10.1016/j.dark.2023.101187. doi:10.1016/j.dark.2023.101187.

[60] Hwang Jc, Noh H. On graviton-photon conversions in magnetic environments; 2024.

[61] Hwang Jc, Noh H. Definition of electric and magnetic fields in curved spacetime. Annals of Physics. 2023 Jul;454:169332. Available from: http://dx.doi.org/10.1016/j.aop.2023.169332. doi:10.1016/j.aop.2023.169332.

[62] Ejlli D. Graviton-photon mixing. Exact solution in a constant magnetic field. Journal of High Energy Physics. 2020 Jun;2020(6). Available from: http://dx.doi.org/10.1007/JHEP06(2020)029. doi:10.1007/jhep06(2020)029.

[63] Ellis GFR, Maartens R, MacCallum MAH. Relativistic Cosmology. Cambridge University Press; 2012.

[64] Domcke V, Garcia-Cely C. Potential of Radio Telescopes as High-Frequency Gravitational Wave Detectors. Physical Review Letters. 2021 Jan;126(2). Available from: http://dx.doi.org/10.1103/PhysRevLett.126.021104. doi:10.1103/physrevlett.126.021104.

[65] Domcke V, Garcia-Cely C. Supplementary Material for "Potential of Radio Telescopes as High-Frequency Gravitational Wave Detectors"; 2021. Available from: http://link.aps.org/supplemental/10.1103/PhysRevLett.126.021104. doi:10.1103/physrevlett.126.021104.

[66] Brezin E, Itzykson C. Polarization Phenomena in Vacuum Nonlinear Electrodynamics. Phys Rev D. 1971 Jan;3:618-21. Available from: https://link.aps.org/doi/10.1103/PhysRevD.3.618. doi:10.1103/PhysRevD.3.618.

[67] Ejlli D. Graviton-photon mixing. Exact solution in a constant magnetic field. Journal of High Energy Physics. 2020 Jun;2020(6). Available from: http://dx.doi.org/10.1007/JHEP06(2020)029. doi:10.1007/jhep06(2020)029.

[68] Ramazanov S, Samanta R, Trenkler G, Urban F. Shimmering gravitons in the gamma-ray sky. Journal of Cosmology and Astroparticle Physics. 2023 Jun;2023(06):019. Available from: http://dx.doi.org/10.1088/1475-7516/2023/06/019. doi:10.1088/1475-7516/2023/06/019.

[69] Heisenberg W, Euler H. Consequences of Dirac Theory of the Positron; 2006. Available from: https://arxiv.org/abs/physics/0605038.

[70] Schwinger J. On Gauge Invariance and Vacuum Polarization. Phys Rev. 1951 Jun;82:664-79. Available from: https://link.aps.org/doi/10.1103/PhysRev.82.664. doi:10.1103/PhysRev.82.664.

[71] Raffelt G, Stodolsky L. Mixing of the photon with low-mass particles. Phys Rev D. 1988 Mar;37:1237-49. Available from: https://link.aps.org/doi/10.1103/PhysRevD.37.1237. doi:10.1103/PhysRevD.37.1237.

[72] Damian E. Gravitational waves from the early universe and their detection. Ferrera, Italy: University of Ferrara; 2013. Doctoral dissertation. Available from: https://iris.unife.it/handle/11392/2388876?mode=full.716.

[73] He Y, Giri SK, Sharma R, Mtchedlidze S, Georgiev I. Inverse Gertsenshtein effect as a probe of high-frequency gravitational waves; 2024. Available from: https://arxiv.org/abs/2312.17636.

[74] Lella A, Calore F, Carenza P, Mirizzi A. Constraining gravitational-wave backgrounds from conversions into photons in the Galactic magnetic field; 2024. Available from: https://arxiv.org/abs/2406.17853.

[75] Hernandez P. Neutrino physics. CERN Yellow Reports. 2016:Vol 5 (2016): Proceedings of the 2015 CERN. Available from: https://e-publishing.cern.ch/index.php/CYR/article/view/434. doi:10.5170/CERN-2016-005.85.

[76] Dandoy V, Bertólez-Martínez T, Costa F. High Frequency Gravitational Wave Bounds from Galactic Neutron Stars; 2024. Available from: https://arxiv.org/abs/2402.14092.

[77] Neronov A, Vovk I. Evidence for Strong Extragalactic Magnetic Fields from Fermi Observations of TeV Blazars. Science. 2010 Apr;328(5974):73–75. Available from: http://dx.doi.org/10.1126/science.1184192. doi:10.1126/science.1184192.

[78] Takahashi K, Mori M, Ichiki K, Inoue S, Takami H. LOWER BOUNDS ON MAGNETIC FIELDS IN INTERGALACTIC VOIDS FROM LONG-TERM GeV–TeV LIGHT CURVES OF THE BLAZAR MRK 421. The Astrophysical Journal Letters. 2013 jun;771(2):L42. Available from: https://dx.doi.org/10.1088/2041-8205/771/2/L42. doi:10.1088/2041-8205/771/2/L42.

[79] Ade PAR, et al. Planck 2015 results. XIX. Constraints on primordial magnetic fields. Astron Astrophys. 2016;594:A19. doi:10.1051/0004-6361/201525821.

[80] Vazza F, Brunetti G, Brüggen M, Bonafede A. Resolved magnetic dynamo action in the simulated intracluster medium. Monthly Notices of the Royal Astronomical Society. 2017 11;474(2):1672-87. Available from: https://doi.org/10.1093/mnras/stx2830. doi:10.1093/mnras/stx2830.

[81] Sanders JS. High-resolution X-ray spectroscopy of clusters of galaxies; 2023. Available from: https://arxiv.org/abs/2301.12791.

[82] Mtchedlidze S, Domínguez-Fernández P, Du X, Schmidt W, Brandenburg A, Niemeyer J, et al. Inflationary and Phase-transitional Primordial Magnetic Fields in Galaxy Clusters. The Astrophysical Journal. 2023 Feb;944(1):100. Available from: http://dx.doi.org/10.3847/1538-4357/acb04d. doi:10.3847/1538-4357/acb04d.

[83] Goldreich P, Julian WH. Pulsar Electrodynamics. . 1969 Aug;157:869. doi:10.1086/150119.

[84] Pagano L, Salvati L, Melchiorri A. New constraints on primordial gravitational waves from Planck 2015. Physics Letters B. 2016 Sep;760:823–825. Available from: http://dx.doi.org/10.1016/j.physletb.2016.07.078. doi:10.1016/j.physletb.2016.07.078.

[85] Aghanim N, Akrami Y, Ashdown M, Aumont J, Baccigalupi C, Ballardini M, et al. Planck2018 results: VI. Cosmological parameters. Astronomy amp; Astrophysics. 2020 Sep;641:A6. Available from: http://dx.doi.org/10.1051/0004-6361/201833910. doi:10.1051/0004-6361/201833910.

[86] Fixsen DJ, Kogut A, Levin S, Limon M, Lubin P, Mirel P, et al. ARCADE 2 MEASUREMENT OF THE ABSOLUTE SKY BRIGHTNESS AT 3-90 GHz. The Astrophysical Journal. 2011 May;734(1):5. Available from: http://dx.doi.org/10.1088/0004-637X/734/1/5. doi:10.1088/0004-637x/734/1/5.

[87] Bowman JD, Rogers AEE, Monsalve RA, Mozdzen TJ, Mahesh N. An absorption profile centred at 78 megahertz in the sky-averaged spectrum. Nature. 2018 Mar;555(7694):67–70. Available from: http://dx.doi.org/10.1038/nature25792. doi:10.1038/nature25792.

[88] Amodeo S, Battaglia N, Schaan E, Ferraro S, Moser E, Aiola S, et al. Atacama Cosmology Telescope: Modeling the gas thermodynamics in BOSS CMASS galaxies from kinematic and thermal Sunyaev-Zel'dovich measurements. Phys Rev D. 2021 Mar;103:063514. Available from: https://link.aps.org/doi/10.1103/PhysRevD.103.063514. doi:10.1103/PhysRevD.103.063514.

[89] Peccei RD. The Strong CP problem and axions. Lect Notes Phys. 2008;741:3-17. doi:10.1007/978-3-540-73518-2_1.

[90] Peccei RD, Quinn HR. Constraints Imposed by CP Conservation in the Presence of Instantons. Phys Rev D. 1977;16:1791-7. doi:10.1103/PhysRevD.16.1791.

[91] Ejlli A, Ejlli D, Cruise AM, Pisano G, Grote H. Upper limits on the amplitude of ultra-high-frequency gravitational waves from graviton to photon conversion. Eur Phys J C. 2019;79(12):1032. doi:10.1140/epjc/s10052-019-7542-5.

[92] Domcke V, Garcia-Cely C, Rodd NL. Novel Search for High-Frequency Gravitational Waves with Low-Mass Axion Haloscopes. Phys Rev Lett. 2022;129(4):041101. doi:10.1103/PhysRevLett.129.041101.

[93] Gorghetto M, Hardy E, Nicolaescu H. Observing invisible axions with gravitational waves. Journal of Cosmology and Astroparticle Physics. 2021 Jun;2021(06):034. Available from: http://dx.doi.org/10.1088/1475-7516/2021/06/034. doi:10.1088/1475-7516/2021/06/034.

[94] Sebastian E. Resonant Cavities for Gravitational Waves. CERN; 2023. Talk.

[95] Berlin A, Blas D, D'Agnolo RT, Ellis SAR, Harnik R, Kahn Y, et al.. MAGO 2.0: Electromagnetic Cavities as Mechanical Bars for Gravitational Waves; 2023. Available from: https://arxiv.org/abs/2303.01518.

[96] Löwenberg R, Moortgat-Pick G. Lorentz Force Detuning in Heterodyne Gravitational Wave Experiments; 2023. Available from: https://arxiv.org/abs/2307.14379.

[97] Arvanitaki A, Geraci AA. Detecting high-frequency gravitational waves with optically-levitated sensors. Phys Rev Lett. 2013;110(7):071105. doi:10.1103/PhysRevLett.110.071105.

[98] Aggarwal N, Winstone GP, Teo M, Baryakhtar M, Larson SL, Kalogera V, et al. Searching for New Physics with a Levitated-Sensor-Based Gravitational-Wave Detector. Phys Rev Lett. 2022 Mar;128:111101. Available from: https://link.aps.org/doi/10.1103/PhysRevLett.128.111101. doi:10.1103/PhysRevLett.128.111101.

[99] Wallace GS, et al. Non-stoichiometric silicon nitride for future gravitational wave detectors. Class Quant Grav. 2024;41(9):095005. doi:10.1088/1361-6382/ad35a1.

[100] Campbell WM, Goryachev M, Tobar ME. The multi-mode acoustic gravitational wave experiment: MAGE. Scientific Reports. 2023 Jun;13(1). Available from: http://dx.doi.org/10.1038/s41598-023-35670-y. doi:10.1038/s41598-023-35670-y.

[101] de Fatis TT. Bulk Acoustic Wave devices for high-frequency gravitational wave antennas. CERN; 2023. Talk.